Daniel Kapeller

# Model Predictive Control for a SCR System

**Master's Thesis**

Graz University of Technology

Institut für Regelungs- und Automatisierungstechnik
Head: Univ.-Prof. Dipl-Ing. Dr.techn. Martin Horn

Supervisor: Univ.-Prof. Dipl-Ing. Dr.techn. Martin Horn

in cooperation with


Supervisor: Dipl.Ing. Alois Danninger and Dipl.Ing. Rafael Candau

Graz, September 2016

## Statutory Declaration

I declare that I have authored this thesis independently, that I have not used other than the declared sources/resources, and that I have explicitly marked all material which has been quoted either literally or by content from the used sources.

Graz, _____ _____

Date Signature

## Eidesstattliche Erklärung

Ich erkläre an Eides statt, dass ich die vorliegende Arbeit selbstständig verfasst, andere als die angegebenen Quellen/Hilfsmittel nicht benutzt, und die den benutzten Quellen wörtlich und inhaltlich entnommenen Stellen als solche kenntlich gemacht habe.

Graz, am _____ _____

Datum Unterschrift

# Abstract

The continuous increase of emission legislation standards for heavy duty diesel engines leads to a higher importance for exhaust gas after-treatment systems. The leading concept meeting the emission standards for nitrogen oxides ($NO_x$) is Selective Catalytic Reduction (SCR). However, further advanced concepts are required to meet the current and future emission legislation. The aim of this thesis is to apply a Model Predictive Control (MPC) to a SCR dosing system based on a copper-zeolite catalyst and to compare this approach with a current PI model based control.
The first part of this work describes the basic principle of the SCR system, the currently used control approach together with the SCR modeling and the MPC. Thus, following steps include the development of a linear and nonlinear MPC algorithm that is applied to the SCR system. Specifically the nonlinear MPC utilizes two different implementations of a successive linerization (SLNMPC). Final tests of the MPC approach contain a Non-Road Stationary Cycle (NRSC) and a Non-Road Transient Cycle (NRTC), for further comparisons to a nonlinear PI-control.
The evaluation of the controller based on the loading of the catalyst showed in the NRTC test case that the nonlinear MPC had a better tracking than the current model based PI control approach with similar control activity, but higher computational costs. However, a better performance led only to small changes in emissions. Therefore a SLNMPC based on the efficiency of $NO_x$ reduction ($DeNOx$) was also considered with a limitation of the ammonia slip.
For transient test cases, the performance of SLNMPC strongly depends on the sampling time of the re-linearization and the system order of the prediction model. Both, a better approximation of the prediction model and a better control performance lead to higher computational costs.

**Deutsch**
Die stetige Verschärfung von Abgasnormen für Dieselmotoren bei Nutzfahrzeugen hat zu einer höheren Wertigkeit von Abgasnachbehandlungssystemen geführt. Das führende Konzept zur Erfüllung der Abgasnormen für Stickoxside ($NO_x$) ist die Selektive Katalytische Reduktion (SCR). Um die Gesetzgebung für Emissionsstandards zu erfüllen, ist der Einsatz modellbasierter Regelungen nötig. Das Ziel dieser Arbeit ist es, eine Modell Prädiktive Regelung (MPR) auf ein SCR Dosiersystem, basierend auf einem Kupfer-Zeolite Katalysator, anzuwenden und einen Vergleich mit einer derzeitig eingesetzten modellbasierten Regelung anzustellen.
Im ersten Teil wird auf das Grundprinzip des SCR Systems, dem aktuellen Regelungs-

ansatz, sowie auf das MPR Konzept eingangen. Danach wird eine lineare und nichtlineare MPR für das SCR System entwickelt. Für den nichtlinearen MPR Algorithmus wird die Methode der sukzessiven Linearisierung (SLNMPR) mit zwei unterschiedlichen Implementierungsarten verwendet. Abschließend wird das MPR Konzept an einem stationären (NRSC) und transienten (NRTC) Testzyklus simuliert und mit einer nichtlinearen PI Regelung verglichen.
Die Auswertung der Regler basierend auf der Ladung des Katalysators zeigte im transienten Test, dass die nichtlineare MPR eine bessere Nachführung an den Sollwert erreichte als der modellbasierte PI Regler bei ähnlicher Regleraktivität, dafür aber höheren Rechenaufwand benötigte. Die bessere Performance der MPR bewirkte jedoch keine wesentliche Änderung der Abgaswerte für $NO_x$. Deshalb wurde zusätzlich eine SLNMPR basierend auf der Effizienz zur $NO_x$ Reduktion ($DeNO_x$) mit einer Beschränkung des Ammoniakschlupfes betrachtet.
Die Performance der SLNMPR hängt stark von der verwendeten Abtastrate für die Linearisierung und der Systemordnung des prädiktiven Modells ab. Sowohl eine bessere Approximation des prädiktiven Modells, als auch eine bessere Performance des Reglers bedeuten einen höheren Rechenaufwand.

# Contents

# Abbreviations, Chemical Species and Symbols

## Abbreviations

| | |
|---|---|
| CI | Compression Ignition |
| CSTR | Continuous Stirred Tank Reactor |
| DOC | Diesel Oxidation Catalyst |
| DPF | Diesel Particulate Filter |
| ECU | Engine Control Unit |
| IAE | Integral Absolute Error |
| ISE | Integral Squared Error |
| ICA | Integrated Control Activity |
| LMPC | Linear Model Predictive Control |
| LNT | Lean $NO_x$ Trap |
| MIMO | Multi Input Multi Output |
| MBC | Model Based Control |
| MPC | Model Predictive Control |
| NMPC | Nonlinear Model Predictive Control |
| NRSC | Non-Road Steady Cycle |
| NRTC | Non-Road Transient Cycle |
| OP | Operating Point |
| SCR | Selective Catalytic Reduction |
| SISO | Single Input Single Output |
| SLNMPC | Successive Linearization Nonlinear Model Predictive Control |

## Chemical Species

| | |
|---|---|
| $(NH_2)_2CO$ | urea |
| $CO$ | carbon monoxide |
| $CO_2$ | carbon dioxide |
| $H_2O$ | water |
| $HC$ | hydrocarbon |
| $HNCO$ | isocyanic acid |
| $N_2$ | nitrogen |
| $NH_3$ | ammonia |
| $NO$ | nitrogen oxide |
| $NO_2$ | nitrogen dioxide |
| $NO_x$ | nitrogen oxide, sum of $NO$ and $NO_2$ |
| $O_2$ | oxygen |
| $PM$ | particulate matter |

## Symbols

| | | |
|---|---|---|
| $\alpha$ | Feed-ratio | $[-]$ |
| $\epsilon_g$ | Open frontal area | $[-]$ |
| $\theta$ | Ammonia surface coverage (loading) | $[-]$ |
| $\Theta_{NH3}$ | Surface density | $[mol/m^2]$ |
| $\overset{*}{m}$ | Mass flow | $[g/s]$ |
| $\overset{*}{n}$ | Molar flow | $[mol/s]$ |
| $a_R$ | Reactive surface area | $[m^2/m^3]$ |
| $c$ | Molar concentration | $[mol/m^3]$ |
| $E$ | Activation temperature of reaction | $[K]$ |
| $K$ | Frequency factor of reaction | $[var.]$ |
| $M$ | Molar weight | $[g/mol]$ |
| $m$ | Mass | $[kg]$ |
| $n$ | Number of CSTR cells | $[-]$ |
| $p$ | Pressure | $[Pa]$ |
| $r$ | Reaction rate | $[kmol/m^2]$ |
| $R$ | Universal gas constant | $[J/(mol \cdot K)]$ |
| $T$ | Temperature | $[K]$ |
| $V$ | Volume | $[m^3]$ |
| $x$ | Mole fraction | $[mol/mol]$ |

# List of Figures

# List of Tables

# 1. Introduction

## 1.1. Motivation

The combustion of an air-fuel mixture causes a high number of pollutants. The main harmful exhaust gas components are nitrogen oxides ($NO_x$), carbon monoxide ($CO$), hydrocarbons ($HC$) and particulate matter ($PM$). Since the Compression Ignition (CI) engines work with excess air during combustion, the related emissions with highest priority are $NO_x$ and $PM$.
In combustion engines $NO_x$ mainly include nitrogen monoxide ($NO$) and nitrogen dioxide ($NO_2$). $NO$ is colorless, odorless and it converts into $NO_2$ in air. However, $NO_2$ is a red-brown, toxic and bad-smelling gas [13].
Due to the development of higher emission legislation standards over the last years and the need for CI engines with less fuel consumption, reduction of nitrogen oxides ($NO_x$) in exhaust gases became more important in the development process of vehicles.

Table 1.1 shows an overview of EU directives for heavy-duty diesel engines. The continuous decrease of emission limits has led to higher importance for exhaust gas after-treatment systems. These emission standards are valid for the European Stationary Cycle (ESC) and European Transient Cycle (ETC), which are based on real road cycle measurements. Since EURO VI, a World Harmonized Stationary Cycle (WHSC) and a Transient Cycle (WHTC) have been introduced to cover typical worldwide driving conditions.

For the reduction of CI engine-out emissions, commonly used after-treatment systems are:

**Diesel Oxidation Catalyst (DOC):**
A DOC has several tasks. The main function of the DOC is the generation of $NO_2$ by the oxidation of $NO$ with $O_2$. This reaction can run in both directions. However, the DOC can only affect the speed of the reaction [5]. The oxidation of $CO$ and $HC$ to carbon dioxide ($CO_2$) and water ($H_2O$) occurs above a certain temperature limit and increases the exhaust gas temperature after the DOC [13]. Furthermore $PM$ emissions are reduced due to the oxidation of $HC$.

| | | | EURO III | EURO IV | EURO V | EURO VI |
|---|---|---|---|---|---|---|
| | | | 2000 | 2005 | 2008 | 2013 |
| ESC,WHSC | $NO_x$ | $[g/kWh]$ | 5.0 | 3.5 | 2.0 | 0.4 |
| | $PM$ | $[g/kWh]$ | 0.10 | 0.02 | 0.02 | 0.01 |
| | $CO$ | $[g/kWh]$ | 2.1 | 1.5 | 1.5 | 1.5 |
| | $HC$ | $[g/kWh]$ | 0.66 | 0.46 | 0,46 | 0.13 |
| | $NH_3$ | $[ppm]$ | | 25 | 25 | 10 |
| ETC,WHTC | $NO_x$ | $[g/kWh]$ | 5.0 | 3.5 | 2.0 | 0.46 |
| | $PM$ | $[g/kWh]$ | 0.16 | 0.03 | 0.03 | 0.01 |
| | $CO$ | $[g/kWh]$ | 5.4 | 4,0 | 4,0 | 4,0 |
| | $HC$ | $[g/kWh]$ | | | | 0.16 |
| | $NH_3$ | $[ppm]$ | | 25 | 25 | 10 |

Table 1.1.: Overview of EU emission standards for heavy duty diesel engines [7]

**Diesel Particulate Filter (DPF):**
DPF are used to filter $PM$ and soot. They can remove $PM$ from the exhaust gas with an efficiency over 95% [13]. A regeneration of DPF has to be done continuously to avoid overloading the filter and back pressure.

**Lean NOx Trap (LNT):**
LNT, also referred to as $NO_x$ adsorber, is a system to reduce $NO_x$ from the exhaust gas of CI engines. $NO_x$ is adsorbed discontinuously under lean engine operation. Periodic $NO_x$ desorption and reduction is done under rich exhaust gas composition. Durable $NO_x$ reduction is about $20 - 70\%$ depending on the system configuration and $NO_x$ storage is limited above $450°C$. Sulfur reduces the $NO_x$ storage capability, therefore a desulfurization or a sulfur free fuel is required [6].

**Selective Catalytic Reduction (SCR):**
SCR is the leading concept for the reduction of $NO_x$ in exhaust gases. State of the art SCR after-treatment systems reach a $NO_x$ reduction efficiency ($DeNOx$ ratio) above 80% [6]. A reactant, ammonia ($NH_3$), is added to the exhausted gas where it reduces $NO_x$. Since not all of the injected $NH_3$ reacts, a part is emitted. Therefore, also $NH_3$ emissions (slip) have been regulated since EURO IV in 2005. For a detailed description of the SCR system the reader is referred to chapter 1.2.

New concepts use combinations of LNT-SCR or SCR catalysts coated onto DPF systems. The introduction of Real-World Driving Emissions (RDE), including portable emission monitoring systems, will force the SCR system design and the demand for advanced control [11].

**Control Strategies:**
Open loop control strategies are able to achieve high SCR performances, but require large calibration effort. Due to the increasing $DeNO_x$ efficiency requirements and the high costs for time consuming test bed measurements, model based and closed loop control approaches for SCR systems are used to establish new strategies for emission reduction [17]. In chapter 2, a current control strategy is presented.

In order to meet current and future emission legislation, an advanced control concept is investigated in this thesis. Model predictive control (MPC) offers new capabilities, including prediction of future process behavior, optimization of the control action and consideration of system constraints. Chapter 4 will show a method how a MPC could be implemented for a SCR system.

## 1.2. SCR System

### 1.2.1. Basic Principle

In SCR systems, a solution with 32.5% urea in water, commercially called AdBlue, is used as reducing agent to reduce the $NO_x$ concentration in the exhausted gas. To describe to basic structure of the SCR system, it can be divided into two parts, presented in figure 1.1. In the first part, AdBlue is injected into the tailpipe and decomposes to ammonia. Then the reduction of $NO_x$ into nitrogen ($N_2$) and water ($H_2O$) in the SCR catalyst is done in the second part.

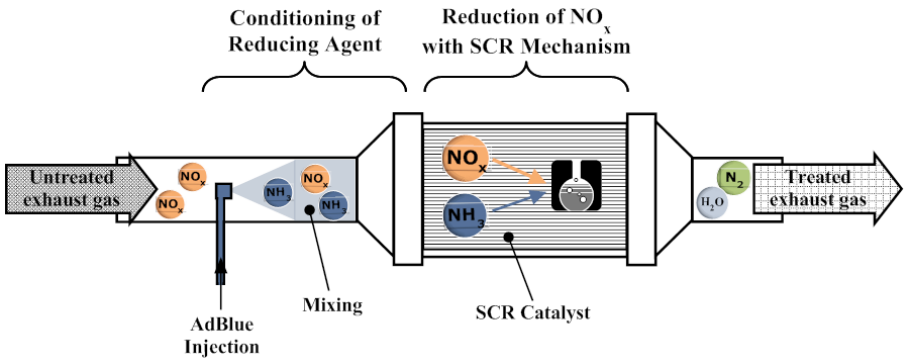


Figure 1.1.: Basic structure of SCR catalyst [15]

The dominant chemical reactions in a SCR aftertreatment system are shown in figure 1.2. As already mentioned, the reducing agent ammonia has to be build out of urea. First the injected AdBlue vaporizes in the tailpipe immediately. The melting

urea ($(NH_2)_2CO$) particles decompose due to thermolysis into ammonia ($NH_3$) and isocyanic acid ($HNCO$). Furthermore the isocyanic acid in combination with water (hydrolysis) is decomposed into $NH_3$ and $CO_2$. The combination of both reactions show that with one molecule urea, two molecules ammonia are produced. It has to be considered that the conversion of urea into ammonia can not take place under the temperature of its melting point (132.7 - 135°C) [8]. Hence, AdBlue should not be injected below this temperature.

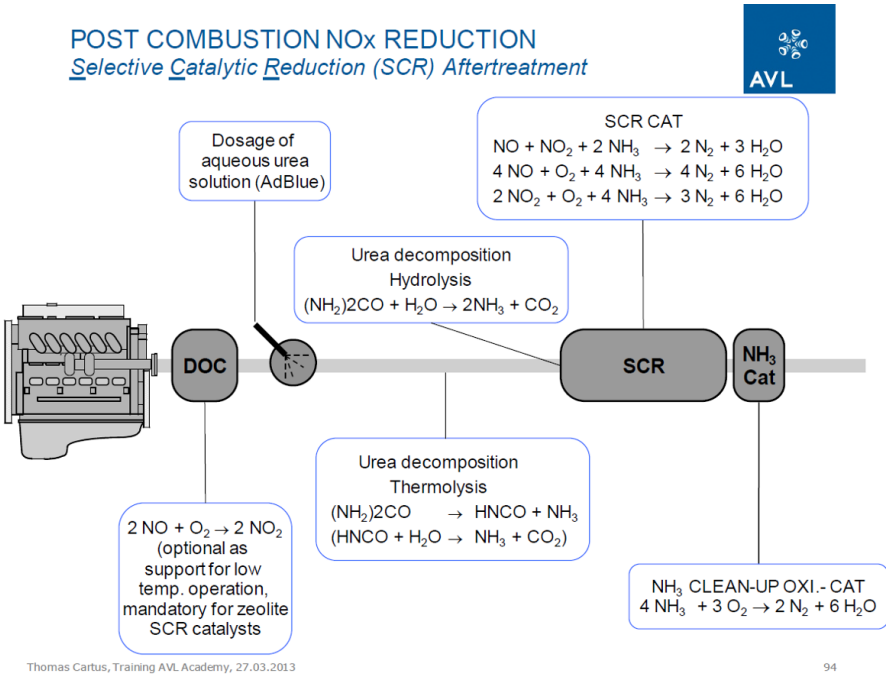


Figure 1.2.: Chemical Reactions in a SCR after-treatment system [6]

In the second part, the obtained ammonia deposits on the surface of the SCR catalyst, which is called ammonia surface coverage or loading of the catalyst. The reduction of the nitrogen oxides $NO$ and $NO_2$ by the ammonia surface coverage leads to the desired products $N_2$ and $H_2O$. This SCR mechanism can be described with three main reactions:

- *Standard SCR Reaction:*

$$4NO + O_2 + 4NH_3 \rightarrow 4N_2 + 6H_2O \tag{1.1}$$

- *Fast SCR Reaction:*

$$NO + NO_2 + 2NH_3 \rightarrow 2N_2 + 3H_2O \tag{1.2}$$

- *Slow SCR Reaction:*

$$2NO_2 + O_2 + 4NH_3 \rightarrow 3N_2 + 6H_2O \tag{1.3}$$

In the Standard SCR reaction 1.1 only $NO$ is reduced. The ratio of $NO_2/NO_x$ is between $0-30\%$ in the exhaust gas. Thus the fast SCR reaction 1.2 also takes place until all $NO_2$ is consumed. The remaining $NO$ is converted by reaction 1.1 [14]. Reaction 1.2 reduces one mole $NO$ and $NO_2$ with one mole $NH_3$ and is about ten times faster than reaction 1.1. Therefore it is the preferred kinetic reaction. For the promotion of the fast reaction, a DOC is used to form more $NO_2$. If high $NO_2/NO_x$ ratios occur in the exhaust gas upstream of the SCR catalyst, the slow reaction 1.3 dominates. Hence a ratio of $NO_2/NO_x > 50\%$ is not desired as it cases the slowest reaction.
Furthermore, if too much ammonia is injected or stored ammonia in the SCR catalyst is released, $NH_3$ emissions (slip) can occur downstream of the catalyst. To reduce this effect, an ammonia slip catalyst (ASC) is applied [11].
For the control approach in this thesis, only the main SCR mechanism is considered.

Typcially, for SCR catalysts vanadia or zeolite based material is used. For the first mobile large scale SCR applications (EURO IV), vanadia catalysts were used due to the experience with stationary diesel engines. According to [11], vanadia-SCR are the cheapest catalysts but with poor durability at high temperatures. Copper zeolite based catalysts have the best low-temperature performance and therefore copper zeolite is the preferred material for SCR applications. Iron zeolite has the best high temperature performance, but a DOC is needed because of its bad behavior at small $NO_2/NO_x$ ratios.

### 1.2.2. Important System Values

An important system value of the SCR is the molar feed-ratio $\alpha$. It is defined as molar ratio between dosed $NH_3$ and exhausted $NO_x$ upstream.

$$\alpha = \frac{\overset{*}{n}_{NH_3,us}}{\overset{*}{n}_{NO_x,us}} \tag{1.4}$$

With the relation $x_i = \frac{\overset{*}{n}_i}{\overset{*}{n}_{EG}}$ the feed-ratio can be rewritten as

$$\alpha = \frac{x_{NH_3,us}}{x_{NO_x,us}} \tag{1.5}$$

where $x_i$ is the amount of substance fraction and can be obtained from an engine-out $NO_x$ model or a $NO_x$ sensor. The feedratio is used as main input for the following

considerations of the SCR system. If ideal conditions are assumed (no $NH_3$ slip, oxidation or other side reactions), a value of $\alpha = 1$ means a 100% reduction of $NO_x$ for the standard SCR reaction.

In order to obtain the amount of injected ammonia, the massflow $\overset{*}{m}_{NH_3}$ upstream of the SCR catalyst is calculated with

$$\overset{*}{n}_{NH_3,us} = \alpha \cdot \overset{*}{n}_{NO_x,us} \tag{1.6}$$

and the relations

$$\overset{*}{n}_{NO_x,us} = \frac{\overset{*}{m}_{EG}}{M_{Air}} \cdot x_{NO_x,us} \tag{1.7}$$

$$\overset{*}{n}_{NH_3,us} = \frac{\overset{*}{m}_{NH_3}}{M_{NH_3}} \tag{1.8}$$

where $\overset{*}{m}_{EG}$,$\overset{*}{m}_{NH_3}$ are the massflows of the exhausted gas and injected $NH_3$, and $M_{Air}$, $M_{NH_3}$ are the molar weights of air and $NH_3$. By substitution the massflow of injected ammonia

$$\overset{*}{m}_{NH_3} = \alpha \cdot \frac{\overset{*}{m}_{EG}}{M_{Air}} \cdot x_{NO_x,us} \cdot M_{NH_3} \tag{1.9}$$

is obtained.

Figure 1.3 shows a scheme of all relevant input and output values of the SCR system, as well as the considered internal states.

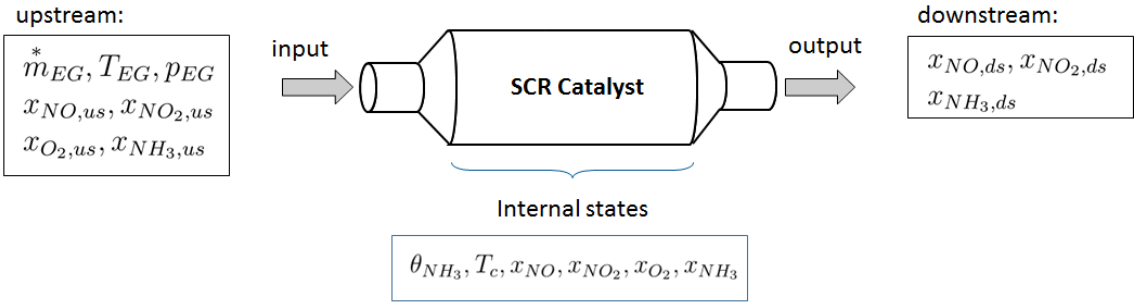


Figure 1.3.: SCR scheme of input, output values and internal states

The important internal states of the SCR catalyst are:

- Catalyst Temperature $T_c$: strongly effects SCR behavior, $NH_3$ storage capability and $DeNO_x$ ratio of the catalyst

- Ammonia surface coverage (loading) $\theta_{NH_3}$: indicates the amount of stored $NH_3$ in the catalyst and thus $NO_x$ reduction efficiency and $NH_3$ slip
- Amount of substance fraction $x$ of the gas species $NO, NO_2, NH_3, O_2$

Input values of the SCR catalyst are the upstream concentrations of the four gas species $NO, NO_2, NH_3, O_2$ as well as the massflow $\overset{*}{m}_{EG}$, temperature $T_{EG}$ and pressure $p_{EG}$ of the exhausted gas. Instead of the concentration $x_{NH_3,us}$, the feedratio $\alpha$ can be used as input (see equation 1.5).

Important values for the evaluation of the SCR performance are the $DeNO_x$ ratio, which is defined as

$$\eta_{NO_x} = \frac{x_{NO_x,us} - x_{NO_x,ds}}{x_{NO_x,us}}, \tag{1.10}$$

as well as the mole fraction $x_{NO_x,ds}$ and the ammonia slip $x_{NH_3,ds}$ downstream of the catalyst.

# 2. State of the Art

The control approach in this thesis is based on the currently used control strategy. Therefore the state of the art is described in the following chapter.

## 2.1. Model Based Control Strategy

### 2.1.1. Control Structure

The model based control (MBC) concept of the SCR system is based on the control of the ammonia surface coverage $\theta_{NH_3}$ (loading of the catalyst).
Figure 2.1 shows the stationary input/output behavior of the SCR system in one operating point (OP). If $\alpha$ increases, which means more ammonia is injected upstream of the catalyst, the amount of $NO_{x,ds}$ downstream decreases. Above an $\alpha$ around one, the steady state loading of the catalyst starts to increase strongly, leading to an increased $NH_3$ slip. As both $NO_{x,ds}$ and $NH_{3,ds}$ are affected by the loading, $\theta_{NH_3}$ is the control variable in the MBC. For every desired stationary tradeoff between $NO_x$ conversion and $NH_3$ slip, an optimal feedratio $\alpha$ can be determined and hence the setpoint for the loading.
For transient conditions, the optimal feedratio differs from its steady state value. In this case the best performance is achieved by reaching the stationary ammonia surface coverage level as fast and best as possible [8].

In figure 2.2, the complete MBC concept is depicted. The engine-out emission model calculates necessary system values from measured sensor data from the exhausted gas of the engine. The output values of the model describe the current operating point of the SCR system. In the observer, a SCR model estimates the internal states of the real SCR catalyst, because non of them are directly measurable. The current value of the loading $\theta_{NH_3}$ is compared with its set-point. The demand of $\theta_{NH_3}$ is calculated as follows. Stationary input/output behavior of the SCR system is simulated and the desired tradeoff of $NO_{x,ds}$ and $NH_{3,ds}$ determines the optimal loading $\theta_{NH_3}$. This procedure is done for several operating points and through interpolation a map can be constructed to cover the whole operation region, depicted in figure 2.3. With increasing catalyst temperature $T_c$ and space velocity $v_s$ the storage capability of the SCR catalyst decreases.

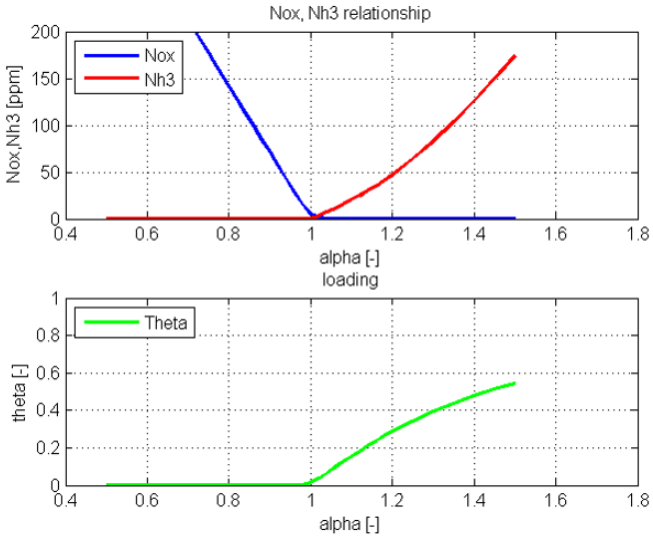


Figure 2.1.: Stationary SCR Input/Output behavior - OP7

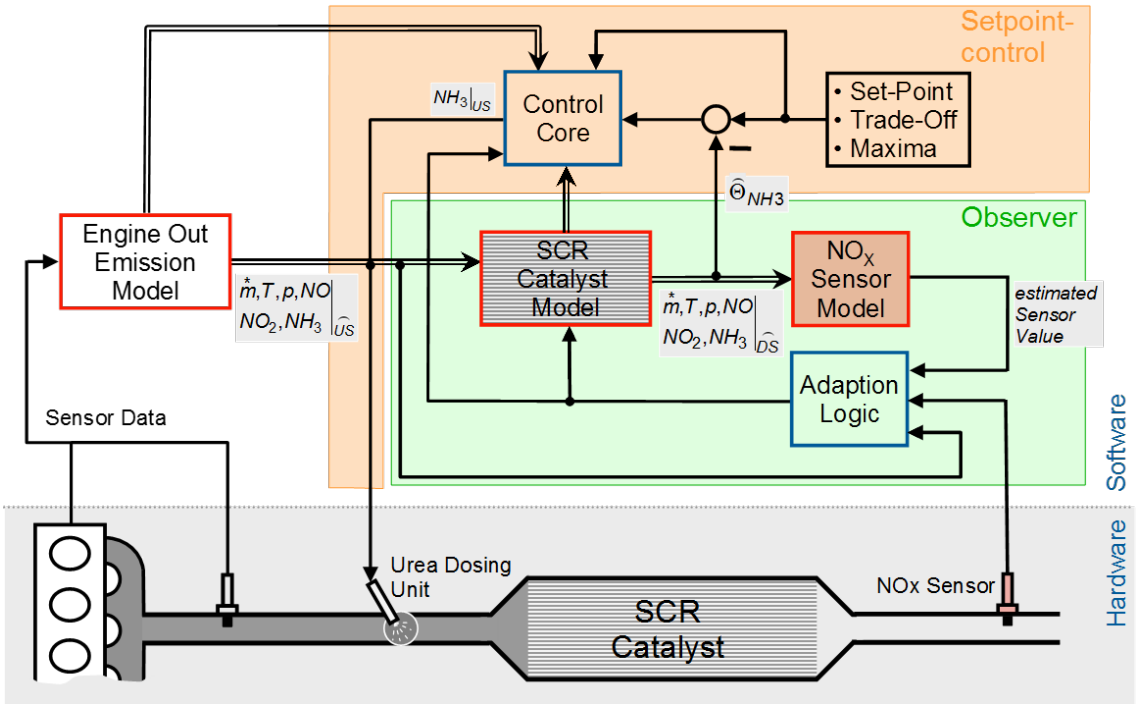


Figure 2.2.: Model based control concept [6]

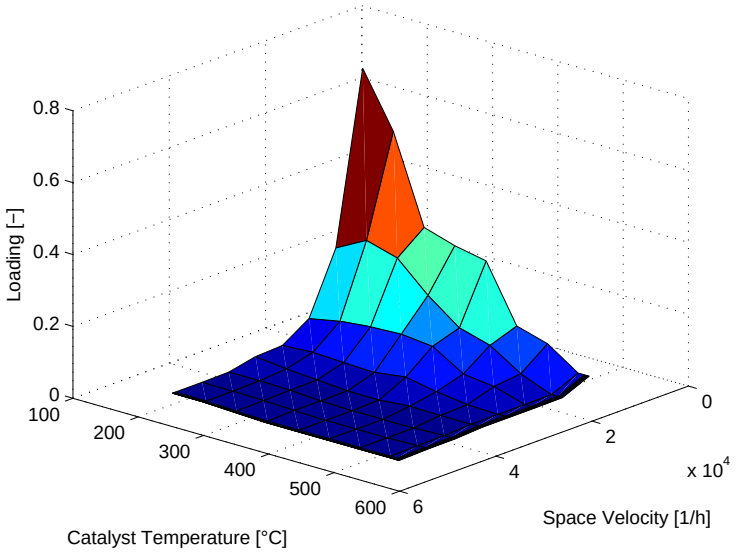


Figure 2.3.: Example of a loading demand map

The loading controller calculates the demand for $NH_{3,us}$, which is converted into an injected AdBlue mass flow. As standard controller a PI with anti windup is used. The setpoint trajectory depends on the current operating point conditions of the system. Due to the changing system properties in different operating points, the parameters of the PI-controller are also changing. Therefore, a set of OP´s which describe the whole operating range are used to generate a map for the control parameters.
Table 2.1 shows a list of 30 operating points that cover the operating range of a considered heavy duty diesel engine.

### 2.1.2. SCR Model

The most sophisticated part of the MBC strategy is the SCR catalyst model. Since this model is also used for the model predictive approach in chapter 4, it is described in greater detail now.

According to [8] and AVL internal research, a plug flow reactor (PFR) would be a proper reactor model for the SCR catalyst. However, a PFR model is based on partial differential equations for the mass balance and is therefore not suitable for a model based control approach embedded in an engine control unit (ECU). Alternatively, the PFR can be approximated using a cascade of continuous stirred tank reactors (CSTR). A schematic of the CSTR cascade is shown in figure 2.4. Here, the SCR model is split into cells, in which each cell represents a CSTR model. Due

| OP | $n$ | $M$ | $\dot{m}^*_{EG}$ | $x_{NO,us}$ | $x_{NO_2,us}$ | $T_{EG}$ | $T_{amb}$ | $p_{EG}$ | $x_{O_2,us}$ |
|---|---|---|---|---|---|---|---|---|---|
| *no.* | $1/min$ | $Nm$ | $kg/h$ | $ppm$ | $ppm$ | $°C$ | $°C$ | $hPa$ | $ppm$ |
| 1 | 1200 | 60 | 320 | 131 | 12 | 168 | 25 | 970 | 183724 |
| 2 | 1200 | 110 | 327 | 162 | 40 | 193 | 25 | 970 | 176066 |
| 3 | 1200 | 161 | 335 | 191 | 92 | 219 | 25 | 970 | 168996 |
| 4 | 1200 | 211 | 344 | 221 | 156 | 242 | 25 | 970 | 161986 |
| 5 | 1200 | 260 | 348 | 216 | 247 | 281 | 25 | 970 | 163815 |
| 6 | 1200 | 353 | 370 | 246 | 331 | 335 | 25 | 970 | 143167 |
| 7 | 1200 | 463 | 398 | 361 | 347 | 385 | 25 | 970 | 127605 |
| 8 | 1200 | 597 | 424 | 609 | 298 | 439 | 25 | 970 | 132106 |
| 9 | 1200 | 802 | 499 | 1008 | 247 | 487 | 25 | 970 | 95065 |
| 10 | 1200 | 1122 | 605 | 1603 | 172 | 542 | 25 | 970 | 74853 |
| 11 | 1500 | 92 | 414 | 136 | 28 | 197 | 25 | 970 | 176625 |
| 12 | 1500 | 138 | 424 | 153 | 65 | 221 | 25 | 970 | 170390 |
| 13 | 1500 | 184 | 439 | 173 | 105 | 246 | 25 | 970 | 164668 |
| 14 | 1500 | 225 | 451 | 196 | 141 | 265 | 25 | 970 | 159809 |
| 15 | 1500 | 277 | 470 | 211 | 187 | 293 | 25 | 970 | 160628 |
| 16 | 1500 | 369 | 505 | 245 | 240 | 333 | 25 | 970 | 152255 |
| 17 | 1500 | 482 | 555 | 310 | 259 | 380 | 25 | 970 | 144211 |
| 18 | 1500 | 686 | 652 | 545 | 244 | 435 | 25 | 970 | 128452 |
| 19 | 1500 | 1154 | 922 | 951 | 198 | 495 | 25 | 970 | 116289 |
| 20 | 1500 | 1471 | 1064 | 1419 | 202 | 523 | 25 | 970 | 107806 |
| 21 | 2100 | 17 | 616 | 75 | 7 | 187 | 25 | 970 | 183186 |
| 22 | 2100 | 78 | 638 | 116 | 25 | 214 | 25 | 970 | 176762 |
| 23 | 2100 | 136 | 668 | 139 | 52 | 240 | 25 | 970 | 171590 |
| 24 | 2100 | 197 | 696 | 161 | 90 | 273 | 25 | 970 | 167378 |
| 25 | 2100 | 264 | 749 | 193 | 119 | 295 | 25 | 970 | 163992 |
| 26 | 2100 | 445 | 903 | 255 | 177 | 355 | 25 | 970 | 148788 |
| 27 | 2100 | 695 | 1172 | 375 | 192 | 398 | 25 | 970 | 139047 |
| 28 | 2100 | 929 | 1318 | 517 | 179 | 443 | 25 | 970 | 122716 |
| 29 | 2100 | 1113 | 1413 | 711 | 160 | 485 | 25 | 970 | 118121 |
| 30 | 2100 | 1208 | 1457 | 812 | 121 | 521 | 25 | 970 | 115241 |

Table 2.1.: Measured operating points

to the mixing properties of an ideal CSTR, the output conditions of one cell are the input conditions of the following cell.

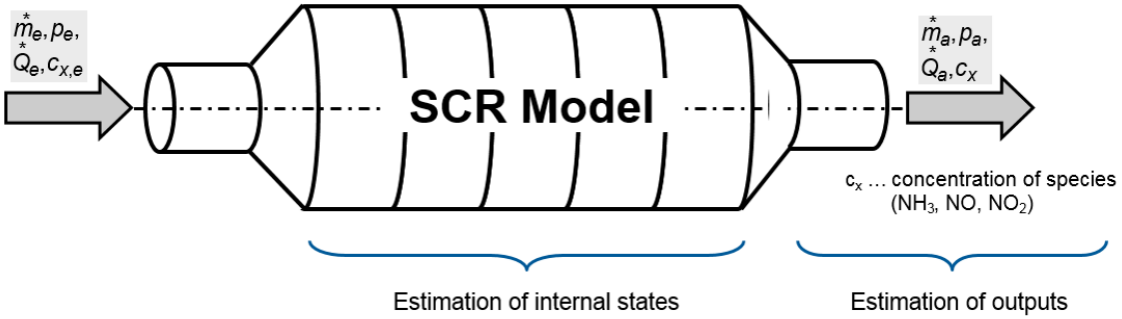


Figure 2.4.: SCR model approach [15]

Additional assumptions and simplifications lead to the entire catalytic converter model of the SCR System. The following model was developed under AVL internal research and published in [8]:

$$
\begin{aligned}
\frac{d}{dt}c_{NO,k} &= \frac{n}{V_c \cdot \epsilon_g} \cdot \frac{\dot{m}^*_{EG} \cdot R}{p_{EG} \cdot M_{EG}}(T_{c,k-1} \cdot c_{NO,k-1} - T_{c,k} \cdot c_{NO,k}) \\
&\quad + a_R(-4 \cdot r_{std,k} - 2 \cdot r_{fst,k} - r_{NO,g,k}) \\
\frac{d}{dt}c_{NO2,k} &= \frac{n}{V_c \cdot \epsilon_g} \cdot \frac{\dot{m}^*_{EG} \cdot R}{p_{EG} \cdot M_{EG}}(T_{c,k-1} \cdot c_{NO2,k-1} - T_{c,k} \cdot c_{NO2,k}) \\
&\quad + a_R(-2 \cdot r_{fst,k} - 6 \cdot r_{slw,k} + r_{NO,g,k}) \\
\frac{d}{dt}c_{NH3,k} &= \frac{n}{V_c \cdot \epsilon_g} \cdot \frac{\dot{m}^*_{EG} \cdot R}{p_{EG} \cdot M_{EG}}(T_{c,k-1} \cdot c_{NH3,k-1} - T_{c,k} \cdot c_{NH3,k}) \\
&\quad + a_R(-r_{ad,k} + r_{de,k} - 4 \cdot r_{ox,g,k}) \\
\frac{d}{dt}c_{O2,k} &= \frac{n}{V_c \cdot \epsilon_g} \cdot \frac{\dot{m}^*_{EG} \cdot R}{p_{EG} \cdot M_{EG}}(T_{c,k-1} \cdot c_{O2,k-1} - T_{c,k} \cdot c_{O2,k}) \\
&\quad + a_R(-0.5 \cdot r_{NO,g,k}) \\
\frac{d}{dt}\theta_{NH3,k} &= \frac{1}{\Theta_{NH3}}(r_{ad,k} - r_{de,k} - 4 \cdot r_{std,k} - 4 \cdot r_{fst,k} - 8 \cdot r_{slw,k} - 4 \cdot r_{ox,k}) \\
\frac{d}{dt}T_{c,k} &= \frac{n}{m_c \cdot c_{p,c}}(\dot{m}^*_{EG} \cdot c_{p,EG}(T_{c,k-1} - T_{c,k}) + \alpha_c \cdot a_c(T_{amb} - T_{c,k}))
\end{aligned}
\tag{2.1}
$$

where $c_i$ is the molar concentration of each gas species ($NO$,$NO_2$,$NH_3$,$O_2$) and $r_i$

are the reaction rates with following relations:

$$
\begin{aligned}
r_{ad} &= K_{ad} \cdot e^{-\frac{E_{ad}}{Tc}} \cdot c_{NH3}(1-\theta_{NH3}) \\
r_{de} &= K_{de} \cdot e^{-\frac{E_{de}(1-\epsilon\cdot\theta_{NH3})}{Tc}} \cdot \theta_{NH3} \\
r_{std} &= K_{std} \cdot e^{-\frac{E_{std}}{Tc}} \cdot c_{NO} \cdot \theta_{crit}(1-e^{-\frac{\theta_{NH3}}{\theta_{crit}}}) \\
r_{fst} &= K_{fst} \cdot e^{-\frac{E_{fst}}{Tc}} \cdot c_{NO} \cdot c_{NO2} \cdot \theta_{crit}(1-e^{-\frac{\theta_{NH3}}{\theta_{crit}}}) \\
r_{slw} &= K_{slw} \cdot e^{-\frac{E_{slw}}{Tc}} \cdot c_{NO2} \cdot \theta_{crit}(1-e^{-\frac{\theta_{NH3}}{\theta_{crit}}}) \\
r_{ox} &= K_{ox} \cdot e^{-\frac{E_{ox}}{Tc}} \cdot \theta_{NH3} \\
r_{ox,g} &= K_{ox,g} \cdot e^{-\frac{E_{ox,g}}{Tc}} \cdot c_{NH3} \\
r_{NO,I} &= K_{NO,I} \cdot T_c^{A_{NO,I}} e^{-\frac{E_{NO,I}}{Tc}} \cdot (c_{NO} \cdot c_{O2}^{0.5} - \frac{c_{NO2}}{K_{equ}(T_c)}) \cdot (1-\theta_{NH3}) \\
r_{NO,II} &= -K_{NO,II} \cdot T_c^{A_{NO,II}} e^{-\frac{E_{NO,II}}{Tc}} \cdot (c_{NO_2} - K_{equ}(T_c) \cdot c_{NO} \cdot c_{O2}^{0.5}) \cdot (1-\theta_{NH3}) \\
r_{NO,g} &= \begin{cases} r_{NO,I} & \text{for } (c_{NO} \cdot c_{O2}^{0.5} - \frac{c_{NO2}}{K_{equ}(T_c)}) \geq 0 \\ r_{NO,II} & \text{for } (c_{NO} \cdot c_{O2}^{0.5} - \frac{c_{NO2}}{K_{equ}(T_c)}) < 0 \end{cases}
\end{aligned}
\tag{2.2}
$$

Equations (2.1), a set of highly nonlinear coupled differential equations, describe the behavior of the SCR catalyst. Index $k$ indicates the set of ordinary differential equations (ODE) for one CSTR cell. For $n$ cells, $n \cdot 6$ equations describe the whole SCR model. In each CSTR cell, material balance, heat balance and SCR reaction kinetics are considered. As formulated in the equations (2.2), the following reactions are taken into account:

- Adsorption and desorption of $NH_3$ on the surface of the SCR catalyst
- Slow, standard and fast SCR reaction mechanism
- Oxidation of $NH_3$ on the catalyst surface and in the gas phase
- Oxidation of $NO_x$

For a better approximation of $NO_x$ oxidation in the model, the reaction rate equation of $r_{NO,I}$ and $r_{NO,II}$ are adjusted with a nonlinear loading term

$$
\begin{aligned}
r_{NO,I} &= K_{NO,I} \cdot T_c^{A_{NO,I}} e^{-\frac{E_{NO,I}}{Tc}} \cdot (c_{NO} \cdot c_{O2}^{0.5} - \frac{c_{NO2}}{K_{equ}(T_c)}) \cdot (1-\theta_{NH3})^a \theta_{NH3}^a \\
r_{NO,II} &= -K_{NO,II} \cdot T_c^{A_{NO,II}} e^{-\frac{E_{NO,II}}{Tc}} \cdot (c_{NO_2} - K_{equ}(T_c) \cdot c_{NO} \cdot c_{O2}^{0.5}) \cdot (1-\theta_{NH3})^a \theta_{NH3}^a
\end{aligned}
\tag{2.3}
$$

where for both equations the equilibrium constant $K_{equ}$ is calculated as

$$K_{equ} = \sqrt{\left(\frac{p_{EG}}{R \cdot T_c}\right)^{-1}} \cdot e^{(-9.259 + \frac{6848}{T_c} + 0.2791 \frac{T_c}{1000} - 0.02245(\frac{T_c}{1000})^2 - 0.4139 \cdot ln(\frac{T_c}{1000}))} \tag{2.4}$$

Under the assumption that parameter $K_{NO,I}$ equals

$$K_{NO,I} = \frac{K_{NO,II}}{K_{equ}} \tag{2.5}$$

reaction rate $r_{NO,I}$ and $r_{NO,II}$ are the same. Therefore, only $r_{NO,I}$ is used as $NO_x$ oxidation term $r_{NO,g}$ for further considerations.

The relation between the molar concentration $c_i$ in $[mol/m^3]$ used in the SCR model and the mole fraction $x_i$ in [ppm] from chapter 1.2.2 of a gas species can be obtained using the ideal gas formula in a rearranged form.

$$\underbrace{\frac{n}{V}}_{c} = \frac{p}{R \cdot T} \tag{2.6}$$

From the formulation $x_i = \frac{c_i}{c}$ follows

$$c_i\left[\frac{mol}{m^3}\right] = \frac{p[pa]}{T[K] \cdot R[\frac{J}{molK}]} x_i\left[\frac{mol}{mol}\right] \tag{2.7}$$

For the implementation of the SCR model in the model based control strategy, the continuous equations are discretized with the *Backward-Euler Method* and linearized in some parts.

# 3. MPC

The following chapter describes how model predictive controller basically work and how they are realized in a state space model. At the end, a linear and nonlinear approach is presented.

## 3.1. Basic Principle

Model predictive control (MPC) describes a control method, in which a model, based on a process system, is used to obtain future control action by minimizing a cost function. Basically, the MPC can be split into three parts:

- prediction model to predict process output at future time instants
- control algorithm to minimize a cost function and obtain future control action
- receding horizon to use past measurements at each time step for the calculation of N future values

The different MPC strategies differ only in the used model and cost function. This concept offers different properties over other control methods [4]:

+ easy tuning
+ usable for different process dynamics, including plants with high complexity, time delay or non-minimum phase
+ easy handling of multivariable case (MIMO systems)
+ systematic implementation of constraints
+ extremely useful if future reference trajectory is known
- high computation time, especially when dealing with constraints and online adaptions
- appropriate model for prediction required

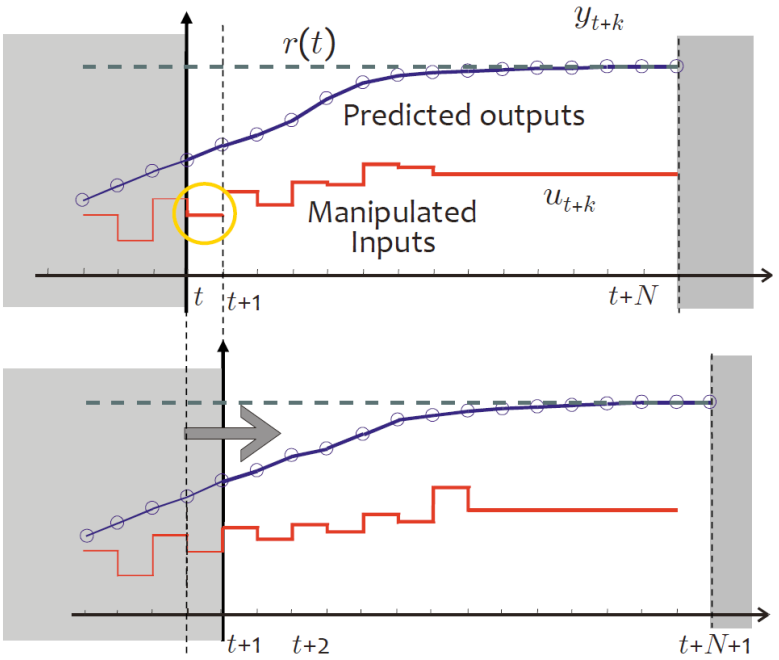


Figure 3.1.: Basic MPC strategy [3]

In figure 3.1 the basic MPC strategy is presented. At each time instant future outputs $y_{t+k}$ for a finite horizon of N steps are calculated using a process model. These future outputs depend on past inputs, past outputs and on future control variables $u_{t+k}$. The set of future control variables is determined by solving an optimal control problem based on a certain cost function to keep the process output as close as possible to a reference trajectory $r(t)$ with minimal control action. Due to the receding horizon concept, only the first future control signal $u_{t+1}$ is sent to the process. At the next time instant $t+1$, new process measurements are available and the future process behavior is calculated again for $N$ steps. The main advantage of the repeated online optimization is the obtained feedback. A general scheme of a MPC controller is shown in figure 3.2.

## 3.2. State Space Notation

A common description for process systems in control theory is the state-space formulation. In discrete time, difference equations describe a state-space model as follows [9]:

$$\begin{aligned} \mathbf{x}_{k+1} &= \mathbf{A}\mathbf{x}_k + \mathbf{b}u_k \\ y_k &= \mathbf{c}^T\mathbf{x}_k \end{aligned} \tag{3.1}$$

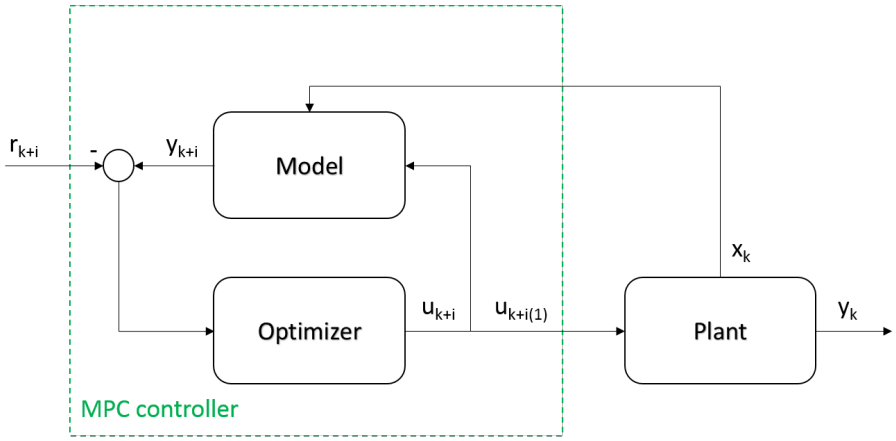


Figure 3.2.: Basic structure of MPC controller

With the $n$-dimensional state vector $\mathbf{x}$ at time instant $k$ and $k+1$, input $u_k$ and ouput $y_k$. In the SISO case $u_k$ and $y_k$ are scalars, $\mathbf{A}$ is a matrix and $\mathbf{b}$ and $\mathbf{c}$ are vectors. If the state space model is extended to the MIMO case, $u_k$ and $y_k$ become vectors and $\mathbf{A}$,$\mathbf{b}$ and $\mathbf{c}$ are matrices. For the following descriptions, only the SISO case is considered.

As a next step, the linear discrete state space model (3.1) has to be used to obtain a prediction model, which calculates future output values over a defined horizon N. One method describes the future output vector $\mathbf{y}_{k+i}^{\rightarrow}$[1] as a function of the current state vector $\mathbf{x}_k$, past input $u_{k-1}$ and unknown future control action increments $\Delta\mathbf{u}_k^{\rightarrow}$, using the relation $u_k = u_{k-1} + \Delta u_k$ and the discrete model [10]. It starts with an iteration of the difference equation

$$\begin{aligned} \mathbf{x}_{k+1} &= \mathbf{A}\mathbf{x}_k + \mathbf{b}u_k \\ \mathbf{x}_{k+2} &= \mathbf{A}\mathbf{x}_{k+1} + \mathbf{b}u_{k+1} \\ &\vdots \\ \mathbf{x}_{k+n_p} &= \mathbf{A}\mathbf{x}_{k+np-1} + \mathbf{b}u_{k+n_c-1} \\ \\ y_{k+n_p} &= \mathbf{c}^T\mathbf{x}_{k+n_p} \end{aligned} \tag{3.2}$$

[1] An arrow denotes the prediction of a system variable

and ends up using trivial matrix-vector formulation in

$$\underset{\rightarrow}{\mathbf{y}}_{k+i} = \begin{bmatrix} \mathbf{c}^T\mathbf{A} \\ \mathbf{c}^T\mathbf{A}^2 \\ \vdots \\ \mathbf{c}^T\mathbf{A}^{np} \end{bmatrix} \mathbf{x}_k + \begin{bmatrix} \mathbf{c}^T\mathbf{b} \\ \mathbf{c}^T(\mathbf{A}+\mathbf{I})\mathbf{b} \\ \vdots \\ \mathbf{c}^T(\mathbf{A}^{n_p-1}+\mathbf{A}^{n_p-2}+..+\mathbf{A}+\mathbf{I})\mathbf{b} \end{bmatrix} u_{k-1} + \begin{bmatrix} \mathbf{c}^T\mathbf{b} & 0 & \cdots & 0 \\ \mathbf{c}^T(\mathbf{A}+\mathbf{I})\mathbf{b} & \mathbf{c}^T\mathbf{b} & \cdots & 0 \\ \vdots & \vdots & \vdots & \vdots \\ \mathbf{c}^T(\mathbf{A}^{n_p-1}+..+\mathbf{I})\mathbf{b} & \mathbf{c}^T(\mathbf{A}^{n_p-2}+..+\mathbf{I})\mathbf{b} & \cdots & \mathbf{c}^T(\mathbf{A}^{n_p-nc}+..+\mathbf{I})\mathbf{b} \end{bmatrix} \underset{\rightarrow}{\Delta\mathbf{u}}_k \tag{3.3}$$

with

$$\underset{\rightarrow}{\mathbf{y}}_{k+i} = \begin{bmatrix} y_{k+1} \\ y_{k+2} \\ \vdots \\ y_{k+np} \end{bmatrix}, \quad \underset{\rightarrow}{\Delta\mathbf{u}}_k = \begin{bmatrix} \Delta u_k \\ \Delta u_{k+1} \\ \vdots \\ \Delta u_{k+nc-1} \end{bmatrix}.$$

The length of the future output vector $\underset{\rightarrow}{\mathbf{y}}_{k+i}$ is determined by the prediction horizon $n_p$, the length of the future control action increments $\underset{\rightarrow}{\Delta\mathbf{u}}_k$ by the control horizon $n_c$. If the state vector $\mathbf{x}_k$ is not measurable, a state observer is needed. A matrix notation is given by:

$$\underset{\rightarrow}{\mathbf{y}}_{k+i} = \mathbf{F}\mathbf{x}_k + \mathbf{G}u_{k-1} + \mathbf{H}\underset{\rightarrow}{\Delta\mathbf{u}}_k \tag{3.4}$$

Then the control sequence $\underset{\rightarrow}{\Delta\mathbf{u}}_k$ is calculated by minimizing a cost function. There are several types of objective functions used for MPC, a common form is used in [10],

$$J = (\underset{\rightarrow}{\mathbf{y}}_{k+i} - \underset{\rightarrow}{\mathbf{r}}_{k+i})^T\mathbf{Q}(\underset{\rightarrow}{\mathbf{y}}_{k+i} - \underset{\rightarrow}{\mathbf{r}}_{k+i}) + (\underset{\rightarrow}{\Delta\mathbf{u}}_k)^T\mathbf{R}\underset{\rightarrow}{\Delta\mathbf{u}}_k \tag{3.5}$$

where $\underset{\rightarrow}{\mathbf{r}}_{k+i}$ represents the future trajectory of the setpoint for the prediction length $n_p$. The aim of such a function is that the future output sequence $\underset{\rightarrow}{\mathbf{y}}_{k+i}$ should follow a reference signal in a defined horizon and the control effort $\underset{\rightarrow}{\Delta\mathbf{u}}_k$ should be penalized. The prediction horizon length $n_p$ defines the region where the error of setpoint and future output is penalized. The control horizon $n_c$ always holds $n_c \leq n_p$ and defines the number of future increments $\Delta u$, which are the optimized variables of the cost function. $\mathbf{Q}$ and $\mathbf{R}$ are symmetric weighting matrices and indicate how

strong the terms of the cost function are penalized.

The objective function of equation 3.5 offers four tuning parameters (degrees of freedom):

- prediction horizon $n_p$: the shorter the length, the faster the reaction of the controller
- $n_c$: should be as small as possible, because it indicates the amount of optimization variables. A higher number leads to a better optimization
- $\mathbf{Q}$ and $\mathbf{R}$ matrices: normally, diagonal matrices are used for easier tuning. The $\mathbf{Q}$ matrix penalizes the future output error, the $\mathbf{R}$ matrix penalizes the increments of control action. In the SISO case the Q/R ratio can be used for tuning if $\mathbf{Q}$ has equal entries and $\mathbf{R}$ has equal entries. A higher Q/R ratio means a faster controller with higher changes in control action.

The substitution of the future output equation (3.4) into the cost function leads to the future control sequence by minimizing the cost function. If no constraints are considered and the cost function is in a quadratic form, then an analytical solution exists to calculate the future control sequence. If both horizons become infinity and there are no constraints, the MPC controller becomes a linear quadratic regulator (LQR) [4]. Otherwise, an iterative method of optimization is needed. For a quadratic cost function with linear inequality constraints, the optimization becomes a standard quadratic programming problem. A standard formulation is expressed in [16]

$$\min_{\mathbf{x}} \; J = \frac{1}{2}\mathbf{x}^T\mathbf{H}\mathbf{x} + \mathbf{b}^T\mathbf{x} \quad \text{s.t. } \mathbf{M}\mathbf{x} \leq \mathbf{d} \tag{3.6}$$

with decision variable $\mathbf{x}$ and matrices and vectors $\mathbf{H}, \mathbf{b}, \mathbf{M}, \mathbf{d}$.
Typically, two kinds of constraints are implemented. Concerning the control variable $u_k$ or the output $y_k$ and state variable $\mathbf{x}_k$.
Constraints on the amplitude of the control variable $u_k$ are the most common ones. The transformation of

$$u_{min} \leq u_k \leq u_{max} \tag{3.7}$$

into linear inequalities is based on the decision variable $\Delta u_k$ and expressed as set of equations at future samples. For the SISO case (3.7) is extended to:

$$\begin{aligned} u_{min} \leq u_k &= u_{k-1} + \Delta u_k \leq u_{max} \\ u_{min} \leq u_{k+1} &= u_{k-1} + \Delta u_k + \Delta u_{k+1} \leq u_{max} \\ &\vdots \\ u_{min} \leq u_{k+n_c-1} &= u_{k-1} + \Delta u_k + \cdots + \Delta u_{k+n_c-1} \leq u_{max} \end{aligned} \tag{3.8}$$

Equation (3.7) expressed by two inequalities

$$\begin{aligned} -u_k &\leq -u_{min} \\ u_k &\leq u_{max} \end{aligned} \tag{3.9}$$

leads to the matrix form

$$\begin{bmatrix} -\mathbf{M} \\ \mathbf{M} \end{bmatrix} \underset{\rightarrow}{\Delta \mathbf{u}_k} \leq \begin{bmatrix} -\mathbf{u}_{min} + \mathbf{l}u_{k-1} \\ \mathbf{u}_{max} - \mathbf{l}u_{k-1} \end{bmatrix} \tag{3.10}$$

with

$$\mathbf{M} = \begin{bmatrix} 1 & 0 & \cdots & \cdots & 0 \\ 1 & 1 & 0 & \cdots & 0 \\ \vdots & \vdots & \ddots & & \vdots \\ \vdots & \vdots & & \ddots & 0 \\ 1 & 1 & \cdots & \cdots & 1 \end{bmatrix}, \mathbf{l} = \begin{bmatrix} 1 \\ 1 \\ \vdots \\ \vdots \\ 1 \end{bmatrix}, \mathbf{u}_{min} = \begin{bmatrix} u_{min} \\ u_{min} \\ \vdots \\ \vdots \\ u_{min} \end{bmatrix} \text{ and } \mathbf{u}_{max} = \begin{bmatrix} u_{max} \\ u_{max} \\ \vdots \\ \vdots \\ u_{max} \end{bmatrix}.$$

$\mathbf{M}$ is a ($n_c$ x $n_c$) coefficient matrix and $\mathbf{l}$, $\mathbf{u}_{min}$ and $\mathbf{u}_{max}$ are ($n_c$ x 1) vectors. Then the form of (3.10) is equivalent to the inequality in (3.6). For the implementation of output and state variable constraints, see [4],[10].

## 3.3. Linear and Nonlinear MPC

### 3.3.1. Linear MPC

Linear MPC (LMPC) in general means that a linear prediction model is used for the prediction. The linear model can be obtained by linearizing nonlinear process model equations, by linear approximation using step responses or by input/output measurements.

In this thesis, a given nonlinear physical model,

$$\dot{\mathbf{x}} = \mathbf{f}(\mathbf{x}, u) \tag{3.11}$$

$$y = g(\mathbf{x}, u) \tag{3.12}$$

with an $n$-dimensional state vector $\mathbf{x} = [x_1\ x_2\ \cdots\ x_n]^T$, will be linearized.
Taylor series expansion is a common method for linearizing nonlinear differential equation and is defined for two scalar variables in [2] as

$$f(x,u) = \sum_{s,t=0}^{\infty} \frac{1}{s!t!} \frac{\partial^{s+t}}{\partial x^s \partial u^t} f(x_0, u_0)(x - x_0)^s (u - u_0)^t \tag{3.13}$$

where $x_0$ and $u_0$ are scalar points for the approximation and $f^{(k)}(x_0, u_0)$ are the function derivatives at $x_0, u_0$.

Generally, the Taylor series is calculated at an equilibrium of the system. To calculate the equilibrium, for example the output $y$ can be chosen as point of linearization. Then the equilibrium of state vector $\mathbf{x}_e$ and input $u_e$ are determined by setting $\frac{d\mathbf{x}}{dt} = \mathbf{0}$.

$$\begin{aligned} \mathbf{0} &= \mathbf{f}(\mathbf{x}_e, u_e) \\ y_e &= g(\mathbf{x}_e, u_e) \end{aligned} \tag{3.14}$$

A linear model is obtained if higher order terms of the Taylor series are neglected. The system variables $u$, $\mathbf{x}$ and $y$ can also be interpreted as sum of equilibrium point and deviation of this point

$$\begin{aligned} u &= u_e + \delta u \\ \mathbf{x} &= \mathbf{x}_e + \delta \mathbf{x} \\ y &= y_e + \delta y \end{aligned} \tag{3.15}$$

Now the linear system is described using (3.13) and (3.15).

$$\frac{d\mathbf{x}}{dt} = \underbrace{\frac{d\mathbf{x}_e}{dt}}_{=0} + \frac{d(\delta \mathbf{x})}{dt} = \underbrace{\mathbf{f}(\mathbf{x}_e, u_e)}_{=0} + \underbrace{\frac{\partial \mathbf{f}}{\partial \mathbf{x}}\Big|_{\mathbf{x}_e, u_e}}_{\mathbf{A}_c} (\mathbf{x} - \mathbf{x}_e) + \underbrace{\frac{\partial \mathbf{f}}{\partial u}\Big|_{\mathbf{x}_e, u_e}}_{\mathbf{b}_c} (u - u_e) + \cdots \tag{3.16}$$

$$y = y_e + \delta y = g(\mathbf{x}_e, u_e) + \underbrace{\frac{\partial g}{\partial \mathbf{x}}\Big|_{\mathbf{x}_e, u_e}}_{\mathbf{c}^T} (\mathbf{x} - \mathbf{x}_e) + \underbrace{\frac{\partial g}{\partial u}\Big|_{\mathbf{x}_e, u_e}}_{d} (u - u_e) + \cdots \tag{3.17}$$

If only linear terms are considered, the linear model is obtained as

$$\frac{d(\delta \mathbf{x})}{dt} = \mathbf{A}_c \delta \mathbf{x} + \mathbf{b}_c \delta u \tag{3.18}$$

$$\delta y = \mathbf{c}^T \delta \mathbf{x} \tag{3.19}$$

with $d = 0$, because output $y$ does not directly depend on the input $u$. For the implementation into the MPC algorithm, the linear model has to be discretized. A way to transform the matrix $\mathbf{A}_c$ and vector $\mathbf{b}_c$ of the continuous system into the discrete form is presented in [9]:

Starting from the general solution of a time-continuous system at time $t = T_d$:

$$\mathbf{x}(T_d) = e^{\mathbf{A}_c T_d} \mathbf{x}_0 + \int_0^{T_d} e^{\mathbf{A}_c (T_d - \tau)} \mathbf{b}_c u(\tau) d\tau \tag{3.20}$$

the discrete matrix $\mathbf{A}$ can be defined as

$$\mathbf{A} = e^{\mathbf{A}_c T_d}. \tag{3.21}$$

For a piecewise equidistant constant input function

$$u(\tau) = u_{const} \quad \text{for} \quad 0 \leq t < T_d$$

the discrete vector $\mathbf{b}$ is

$$\mathbf{b} = \int_0^{T_d} e^{\mathbf{A}_c \tau} \mathbf{b}_c d\tau \tag{3.22}$$

and if $\mathbf{A}_c$ is invertible

$$\mathbf{b} = \mathbf{A}_c^{-1}[e^{\mathbf{A}_c T_d} - \mathbf{I}]\mathbf{b}_c \tag{3.23}$$

is valid. Then the future output sequence $\mathbf{y}_{\overrightarrow{k+i}}$ can be calculated for the linear system with equation (3.3). However, the prediction model of the MPC only describes the deviation from the equilibrium. Therefore back-calculation to $u$, $\mathbf{x}$ and $y$ has to be done with equations (3.15).

### 3.3.2. Nonlinear MPC

In some applications a MPC with linear prediction model is not accurate enough for controlling a process, especially when the system is highly nonlinear or the operating point changes in a wide area.
Therefore a nonlinear MPC (NMPC) concept has to be used. Typical NMPC methods are MPC using successive linearization (SLNMPC), nonlinear models with sequential quadratic programming or neuronal net-based models [10]. Due to the fact that a parametrized physical model exists, the focus of this thesis will be on the NMPC using successive linearization.

Using SLNMPC means that a re-linerization of a nonlinear prediction model is done in every or a defined time step. Thus, the optimization problem is reduced to a quadratic program. The properties of this concept are according to [1]

- adaptive prediction model and controller, which can be used for time variant systems
- better approximation of highly nonlinear plants or systems with wide operating range than LMPC
- nonlinear control method, but quadratic optimization problem

– optimal solution is guaranteed
– less computational costs than in other nonlinear MPC methods

In the following, two methods are described for the implementation of successive linearization.

***Method 1 (M1):***
Use the current output $y_k$ as equilibrium $y_e$ and calculate the equilibrium of state vector $\mathbf{x}_e$ and input $u_e$ of the nonlinear system. Then linearize around $\mathbf{x}_e$ and $u_e$ (same structure as in LMPC, chapter 3.3.1). Problems might occur for higher order systems, because the equilibrium has to be computed numerically.

***Method 2 (M2):***
Linearize around the measured state vector $x_k$ and current input $u_{k-1}$. It has to be considered that the offset $\mathbf{f}(\mathbf{x}_k, u_{k-1})$ does not disappear in M2. Therefore, the linearized model has to be written in a new form

$$\frac{d\mathbf{x}}{dt} = \mathbf{f}(\mathbf{x}_k, u_{k-1}) + \underbrace{\frac{\partial \mathbf{f}}{\partial \mathbf{x}}\Big|_{\mathbf{x}_k, u_{k-1}}}_{\mathbf{A}_c}(\mathbf{x} - \mathbf{x}_k) + \underbrace{\frac{\partial \mathbf{f}}{\partial u}\Big|_{\mathbf{x}_k, u_{k-1}}}_{\mathbf{b}_c}(u - u_{k-1}) \tag{3.24}$$

$$y = g(\mathbf{x}_k, u_{k-1}) + \underbrace{\frac{\partial g}{\partial \mathbf{x}}\Big|_{\mathbf{x}_k, u_{k-1}}}_{\mathbf{c}^T}(\mathbf{x} - \mathbf{x}_k) \tag{3.25}$$

with $\mathbf{x}^* = \mathbf{x} - \mathbf{x}_k$ and $u^* = u - u_{k-1}$.
A way to deal with the initial condition $\mathbf{f}_o = \mathbf{f}(\mathbf{x}_k, u_{k-1})$ is described in [1]. The input vector $\mathbf{b}_c$ is augmented by a further column with $\mathbf{f}_o$, which is corresponding to a second constant input.

$$\frac{d\mathbf{x}^*}{dt} = \mathbf{A}_c\mathbf{x}^* + \begin{bmatrix}\mathbf{b}_c & \mathbf{f}_0\end{bmatrix}\begin{bmatrix}u^* \\ 1\end{bmatrix} \tag{3.26}$$

Then the linear model is discretized,

$$\begin{aligned}\mathbf{x}^*_{k+1} &= \mathbf{A}\mathbf{x}^*_k + \begin{bmatrix}\mathbf{b} & \mathbf{\Gamma}_0\end{bmatrix}\begin{bmatrix}u^*_k \\ 1\end{bmatrix} \\ y^*_k &= \mathbf{c}^T\mathbf{x}^*_k\end{aligned} \tag{3.27}$$

where $\mathbf{A}$, $\mathbf{b}$ and $\mathbf{\Gamma}_0$ are the discrete forms of $\mathbf{A}_c$, $\mathbf{b}_c$ and $\mathbf{f}_0$ (see equations 3.21 and 3.23).

Afterwards, the discrete model is rearranged in a form with one input.

$$\begin{aligned}\mathbf{x}^*_{k+1} &= \mathbf{A}\mathbf{x}^*_k + \mathbf{b}u^*_k + \mathbf{\Gamma}_0 \\ y^*_k &= \mathbf{c}^T\mathbf{x}^*_k\end{aligned} \tag{3.28}$$

The real output $y_k$ is obtained from $y_k = y_k^* + g(\mathbf{x}_k, u_{k-1})$.
Then the structure of the future output vector $\underset{\rightarrow}{\mathbf{y}}_{k+i}$ changes slightly compared to the standard MPC formulation in equation (3.3).

$$\begin{aligned}
\underset{\rightarrow}{\mathbf{y}}_{k+i} = & \begin{bmatrix} \mathbf{c}^T\mathbf{A} \\ \mathbf{c}^T\mathbf{A}^2 \\ \vdots \\ \mathbf{c}^T\mathbf{A}^{np} \end{bmatrix} \mathbf{x}_k^* + \begin{bmatrix} \mathbf{c}^T\mathbf{b} \\ \mathbf{c}^T(\mathbf{A}+\mathbf{I})\mathbf{b} \\ \vdots \\ \mathbf{c}^T(\mathbf{A}^{n_p-1} + \mathbf{A}^{n_p-2} + .. + \mathbf{A} + \mathbf{I})\mathbf{b} \end{bmatrix} u_{k-1}^* \\
& + \begin{bmatrix} \mathbf{c}^T\mathbf{b} & 0 & \cdots & 0 \\ \mathbf{c}^T(\mathbf{A}+\mathbf{I})\mathbf{b} & \mathbf{c}^T\mathbf{b} & \cdots & 0 \\ \vdots & \vdots & \vdots & \vdots \\ \mathbf{c}^T(\mathbf{A}^{n_p-1} + .. + \mathbf{I})\mathbf{b} & \mathbf{c}^T(\mathbf{A}^{n_p-2} + .. + \mathbf{I})\mathbf{b} & \cdots & \mathbf{c}^T(\mathbf{A}^{n_p-nc} + .. + \mathbf{I})\mathbf{b} \end{bmatrix} \underset{\rightarrow}{\Delta\mathbf{u}_k^*} \\
& + \begin{bmatrix} \mathbf{c}^T\mathbf{\Gamma}_0 + g(\mathbf{x}_k, u_{k-1}) \\ \mathbf{c}^T(\mathbf{A}+\mathbf{I})\mathbf{\Gamma}_0 + g(\mathbf{x}_k, u_{k-1}) \\ \vdots \\ \mathbf{c}^T(\mathbf{A}^{n_p-1} + \mathbf{A}^{n_p-2} + .. + \mathbf{A} + \mathbf{I})\mathbf{\Gamma}_0 + g(\mathbf{x}_k, u_{k-1}) \end{bmatrix}
\end{aligned} \tag{3.29}$$

with $u_k^* = u_{k-1} + \Delta u_k^*$. In this notation, the output prediction $\underset{\rightarrow}{\mathbf{y}}_{k+i}$ is a real value.

# 4. MPC Based Approach for SCR Control

After discussing the theory of the SCR system and the principle of MPC, a model predictive control concept based on the current control approach for the SCR is investigated in this chapter.

## 4.1. Objectives

The objective of the control approach is to design an MPC concept for an existing SCR system model. Figure 4.1 shows the structure of the MPC strategy, which is based on the MBC control concept in chapter 2 and has to be implemented as a controller in MATLAB Simulink. For the evaluation of the MPC strategy, the SCR model of the observer is used as plant model for the SCR system.

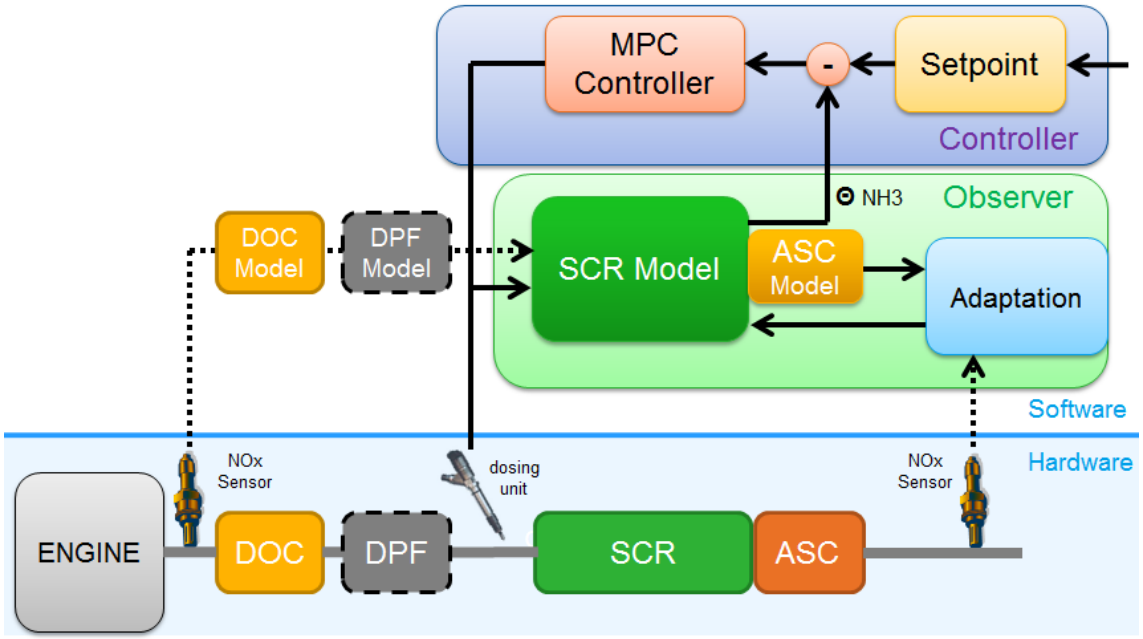


Figure 4.1.: MPC strategy for the SCR system

## 4.2. Investigation of the Continuous SCR Model

As already discussed in chapter 3, the design of an MPC requires a prediction model. The idea is to use the continuous description of the SCR system in equation (2.1) and (2.2) and linearize them to obtain a linear prediction model. In a first step, the continuous nonlinear SCR model has to be built up.

In order to reduce the complexity of the continuous model, only four of the six differential equations for one cell are considered. The states for the catalyst temperature $T_c$ and the concentration of oxygen $c_{O2}$ are set constant, because their influence over the prediction horizon is considered negligible. This assumption will be confirmed later. The reduced continuous model equations for one CSTR cell are

$$\begin{aligned}
\frac{d}{dt}c_{NO,k} &= \frac{n}{V_c \cdot \epsilon_g} \cdot \frac{\overset{*}{m}_{EG} \cdot R}{p_{EG} \cdot M_{EG}}(T_{c,k-1} \cdot c_{NO,k-1} - T_{c,k} \cdot c_{NO,k}) \\
&\quad + a_R(-4 \cdot r_{std,k} - 2 \cdot r_{fst,k} - r_{NO,g,k}) \\
\frac{d}{dt}c_{NO_2,k} &= \frac{n}{V_c \cdot \epsilon_g} \cdot \frac{\overset{*}{m}_{EG} \cdot R}{p_{EG} \cdot M_{EG}}(T_{c,k-1} \cdot c_{NO_2,k-1} - T_{c,k} \cdot c_{NO_2,k}) \\
&\quad + a_R(-2 \cdot r_{fst,k} - 6 \cdot r_{slw,k} + r_{NO,g,k}) \\
\frac{d}{dt}c_{NH_3,k} &= \frac{n}{V_c \cdot \epsilon_g} \cdot \frac{\overset{*}{m}_{EG} \cdot R}{p_{EG} \cdot M_{EG}}(T_{c,k-1} \cdot c_{NH_3,k-1} - T_{c,k} \cdot c_{NH_3,k}) \\
&\quad + a_R(-r_{ad,k} + r_{de,k} - 4 \cdot r_{ox,g,k}) \\
\frac{d}{dt}\theta_{NH3,k} &= \frac{1}{\Theta_{NH3}}(r_{ad,k} - r_{de,k} - r_{std,k} - 4 \cdot r_{fst,k} - 8 \cdot r_{slw,k} - 4 \cdot r_{ox,k})
\end{aligned} \tag{4.1}$$

with the same reaction rates as in equations (2.2) and (2.3) and the assumption $r_{NO,g,k} = r_{NO,I,k}$.

Now the continuous model can be implemented in MATLAB Simulink. For simplification, the following reactions in the SCR system are not considered:

- standard and slow SCR reactions: $r_{std}$, $r_{slw}$
- oxidation of $NH_3$ in the gas phase: $r_{ox,g}$

In order to verify if the modeling of the continuous system is correct, it is compared to the discrete SCR plant. The comparison of the continuous and discrete model is shown with 1 cell in figure 4.2 and with 15 cells in figure 4.3 for input jumps of the feed-ratio $\alpha$ in one operating point (OP7 from table 2.1). In both cases only minor deviations occur.

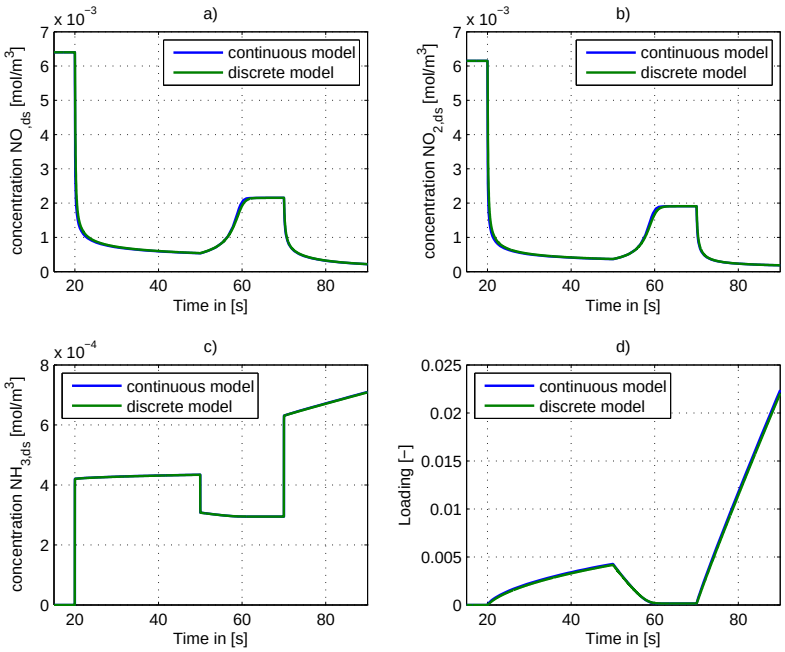


Figure 4.2.: Comparison of continuous and discrete model for 1 cell.

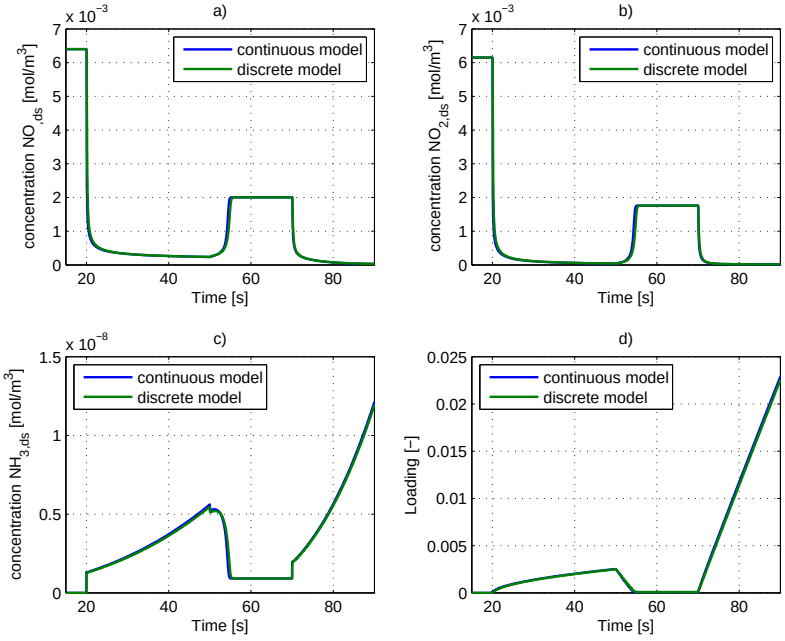


Figure 4.3.: Comparison of continuous and discrete model for 15 cell.

Before the continuous model can be used for further investigations, the assumption of constant $T_c$ and $c_{O2}$ over the prediction horizon has to be proofed. Figure 4.4 shows the SCR model behavior with 15 cells if 5 times more or 0.2 times less $O_2$ than in the normal operating point (OP7) is available. These values represent the amounts of $c_{O_2}$ in the whole operating range. One can see that changes of $c_{O_2}$ from minimal to maximal operating range only lead to small deviations of $NO$, $NO_2$, $NH_3$ concentrations and loading time courses. The reason for that is the lean operating mode of the engine, which leads to excess of air in every operating point.

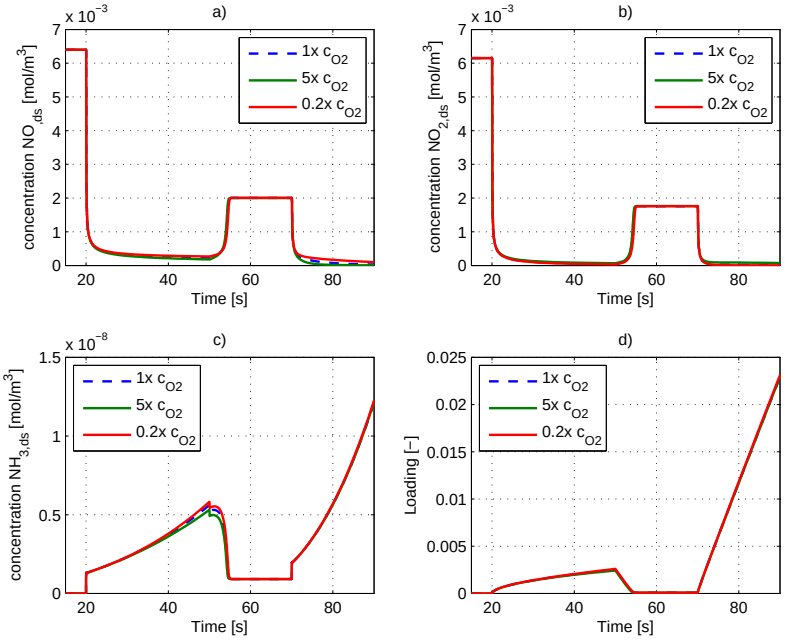


Figure 4.4.: Comparison of deviations of $c_{O_2}$ values from OP7 for the continuous SCR model with 15 cells

Since the temperature of the catalyst changes very slowly, its influence over the prediction horizon should be small. Figure 4.5 depicts the mean catalyst temperature for a transient test. In this case, a maximum change of the temperature $\Delta T_c = 2\frac{K}{s}$ is measured. If a prediction time $T_p = 3s$ is assumed for the MPC, a maximum change of $6K$ can occur during prediction. Figure 4.6 depicts the SCR model behavior with 15 cells for changes in $T_c$ at OP7. Here, the deviations are also small.

Continuous SCR model simulations also contain tests with a different number of cells to define the appropriate system order. Specifically a comparison of the SCR model simulation results based on 2, 6, 8 and 15 cells is depicted in figure 4.7. Internal research of AVL showed that 8 to 15 cells are necessary for a good approximation of the SCR system.

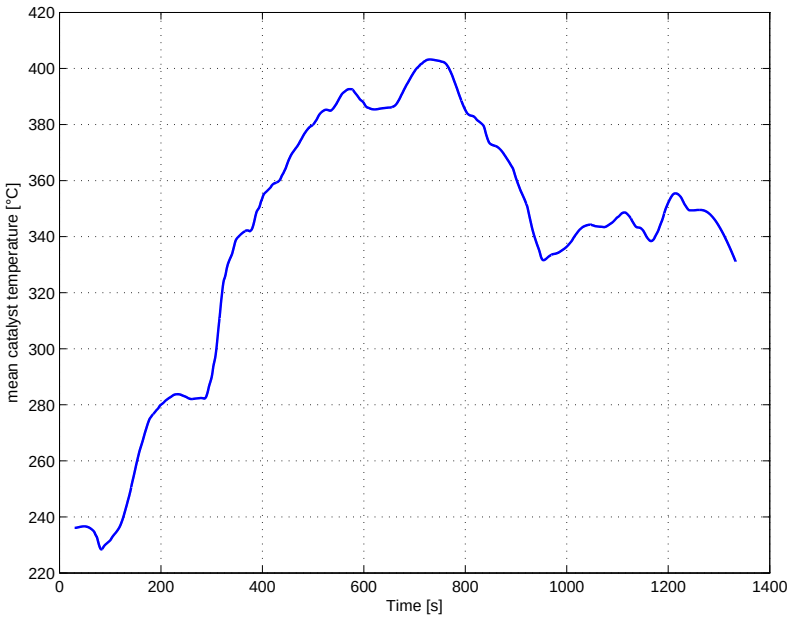


Figure 4.5.: Mean catalyst temperature $T_c$ of a transient test case

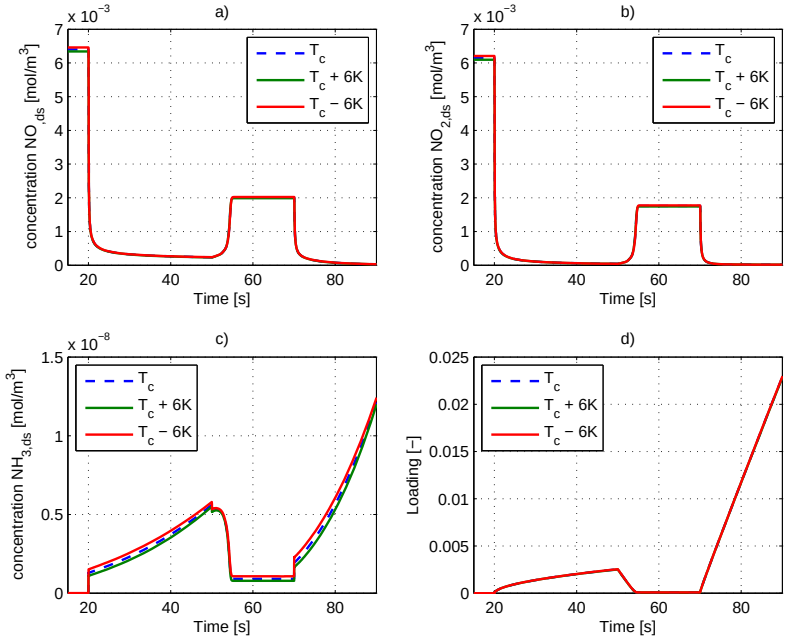


Figure 4.6.: Comparison of deviations of $T_c$ values from OP7 for the continuous SCR model with 15 cells

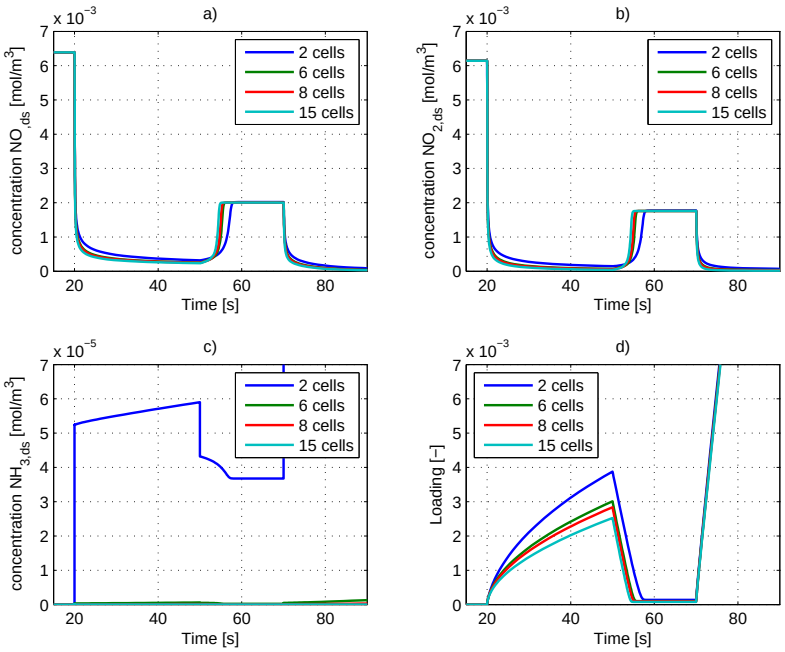


Figure 4.7.: Comparison of different number of cells for the continuous SCR model

## 4.3. Linear MPC for SCR Control

### 4.3.1. Simulation of 1 Cell SCR Model

After the investigation of the continuous model, a simple linear MPC algorithm is tested at the beginning. For the first tests, an SCR model with 1 cell is considered.

In order to obtain a state space model, the state vector $\mathbf{x}$, input $u$ and output $y$ are defined as

$$\begin{aligned} \mathbf{x} &= [x_1\ x_2\ x_3\ x_4]^T = [c_{NO}\ c_{NO2}\ c_{NH3}\ \theta_{NH3}]^T \\ u &= \alpha \\ y &= x_4 \end{aligned} \tag{4.2}$$

where $y$ equals the loading of the catalyst for one CSTR cell.

The differential equations for 1 cell can be rewritten with a state space notation as

follows:

$$\begin{aligned}
\frac{d}{dt}x_1 &= k_1 \cdot \frac{\overset{*}{m}_{EG}}{p_{EG}}(T_{EG} \cdot c_{NO,us} - T_c \cdot x_1) + a_R(-4k_{std} \cdot x_1 \cdot \theta_{crit}(1 - e^{-\frac{x_4}{\theta_{crit}}}) \\
&\quad - 2k_{fst} \cdot x_1 x_2 \cdot \theta_{crit}(1 - e^{-\frac{x_4}{\theta_{crit}}}) - k_{NO,I} \cdot (x_1 \cdot c_{O2}^{0.5} - \frac{x_2}{K_{equ}}) \cdot (1 - x_4)^a x_4^a) \\
\frac{d}{dt}x_2 &= k_1 \cdot \frac{\overset{*}{m}_{EG}}{p_{EG}}(T_{EG} \cdot c_{NO2,us} - T_c \cdot x_2) + a_R(-2k_{fst} \cdot x_1 x_2 \cdot \theta_{crit}(1 - e^{-\frac{x_4}{\theta_{crit}}}) \\
&\quad - 6k_{slw} \cdot x_2 \cdot \theta_{crit}(1 - e^{-\frac{x_4}{\theta_{crit}}}) + k_{NO,I} \cdot (x_1 \cdot c_{O2}^{0.5} - \frac{x_2}{K_{equ}}) \cdot (1 - x_4)^a x_4^a) \\
\frac{d}{dt}x_3 &= k_1 \cdot \frac{\overset{*}{m}_{EG}}{p_{EG}}(T_{EG} \cdot c_{NH_3,us} - T_c \cdot x_3) \\
&\quad + a_R(-k_{ad} \cdot x_3(1 - x_4) + k_{de} \cdot x_4 - 4k_{ox,g} \cdot x_3) \\
\frac{d}{dt}x_4 &= \frac{1}{\Theta_{NH3}}(k_{ad} \cdot x_3(1 - x_4) - k_{de} \cdot x_4 - 4k_{std} \cdot x_1 \cdot \theta_{crit}(1 - e^{-\frac{x_4}{\theta_{crit}}}) \\
&\quad - 4 \cdot k_{fst} \cdot x_1 x_2 \cdot \theta_{crit}(1 - e^{-\frac{x_4}{\theta_{crit}}}) - 8 \cdot k_{slw} \cdot c_{NO2,ds} \cdot \theta_{crit}(1 - e^{-\frac{x_4}{\theta_{crit}}}) - 4 \cdot k_{ox} \cdot x_4)
\end{aligned} \tag{4.3}$$

With constants

$$\begin{aligned}
k_1 &= \frac{n}{V_c \cdot \epsilon_g} \cdot \frac{R}{M_{EG}} \\
k_{std} &= K_{std} \cdot e^{-\frac{E_{std}}{Tc}} \\
k_{fst} &= K_{fst} \cdot e^{-\frac{E_{fst}}{Tc}} \\
k_{slw} &= K_{slw} \cdot e^{-\frac{E_{slw}}{Tc}} \\
k_{ad} &= K_{ad} \cdot e^{-\frac{E_{ad}}{Tc}} \\
k_{de} &= K_{de} \cdot e^{-\frac{E_{de}}{Tc}} \\
k_{ox} &= K_{ox} \cdot e^{-\frac{E_{ox}}{Tc}} \\
k_{ox,g} &= K_{ox,g} \cdot e^{-\frac{E_{ox,g}}{Tc}} \\
k_{NO,I} &= K_{NO,I} \cdot T_c^{A_{NO,I}} \cdot e^{-\frac{E_{NO,I}}{Tc}}
\end{aligned} \tag{4.4}$$

The input $u$ can be introduced by replacing the concentration $c_{NH_3,us}$ with

$$c_{NH_3,us} = (c_{NO,us} + c_{NO2,us}) \cdot \alpha \tag{4.5}$$

since relation (1.5) is also valid for concentrations $c_i$ of the same gas species.

As a next step, a linear MPC controller is tested on the discrete ECU SCR model. For the prediction model, a linearization of equation (4.3) has to be derived. Therefore the nonlinear system (4.3) can be interpreted as vector-valued function $\frac{d\mathbf{x}}{dt} = \mathbf{f}(\mathbf{x}, u)$. As described in chapter 3.3.1, calculating the Jacobian matrices of $\mathbf{f}(\mathbf{x}, u)$ and $g(\mathbf{x}, u)$

$$\frac{\partial \mathbf{f}}{\partial \mathbf{x}} = \begin{bmatrix} \frac{\partial f_1}{dx_1} & \cdots & \frac{\partial f_1}{dx_n} \\ \vdots & \ddots & \vdots \\ \frac{\partial f_m}{\partial x_1} & \cdots & \frac{\partial f_m}{dx_n} \end{bmatrix}, \frac{\partial \mathbf{f}}{du} = \begin{bmatrix} \frac{\partial f_1}{du} \\ \vdots \\ \frac{\partial f_m}{du} \end{bmatrix}, \frac{\partial g}{d\mathbf{x}} = \begin{bmatrix} \frac{\partial g}{\partial x_1} & \cdots & \frac{\partial g}{\partial x_n} \end{bmatrix} \tag{4.6}$$

lead to the matrix $\mathbf{A}_c$ and vectors $\mathbf{b}_c$ and $\mathbf{c}^T$ of the linear continuous model if the equilibrium points are set in.

$$\mathbf{A}_c = \frac{\partial \mathbf{f}}{\partial \mathbf{x}}\Big|_{\mathbf{x}_e, u_e}, \mathbf{b}_c = \frac{\partial \mathbf{f}}{\partial u}\Big|_{\mathbf{x}_e, u_e}, \mathbf{c}^T = \frac{\partial g}{\partial \mathbf{x}}\Big|_{\mathbf{x}_e, u_e} \tag{4.7}$$

The explicit structure of $\mathbf{A}_c$, $\mathbf{b}_c$ and $\mathbf{c}^T$ for one CSTR cell is attached in Appendix A.1. A transformation of the continuous prediction model into a discrete form is obtained using equations (3.21) and (3.23).

The general block diagram of the loading control strategy for the SCR model is depicted in figure 4.8. Internal states of the SCR system are used for the future predictions in the MPC. The current operating point and thus the upstream values of the exhausted gas are depending from the chosen test cycle. The setpoint trajectory of $NH_3$ storage (loading) is determined by the catalyst temperature $T_c$ and massflow of the exhausted gas $\overset{*}{m}_{EG}$.

The SCR catalyst can be wasted if too much $x_{NH_3,us}$ is injected upstream. Therefore, the control variable $\alpha$ is limited to $\alpha = [0.2, 1.5]$, where the lower limit is used to avoid damaging of the catalyst. The implementation of constraints in the MPC is described in chapter 3.2.

Figure 4.9 depicts the simulation of a simple MPC implementation, using only one linear prediction model, linearized about an equilibrium ($y_e = 0.015$) near the desired loading set-point of OP7. The default sample time of the discrete SCR model is $T_s = 0.02s$. Since the computational effort increases strongly for a MPC with increasing $T_s$, it is set to $T_s = 0.1s$ for a start. Then the prediction horizon $n_p$ should be chosen such that the closed loop dynamic is catched. The following parameters are chosen:

$$\begin{aligned} T_s &= 0.1s \\ n_p &= 30 \\ n_c &= 9 \\ T_p &= n_p \cdot T_s = 3s \end{aligned}$$

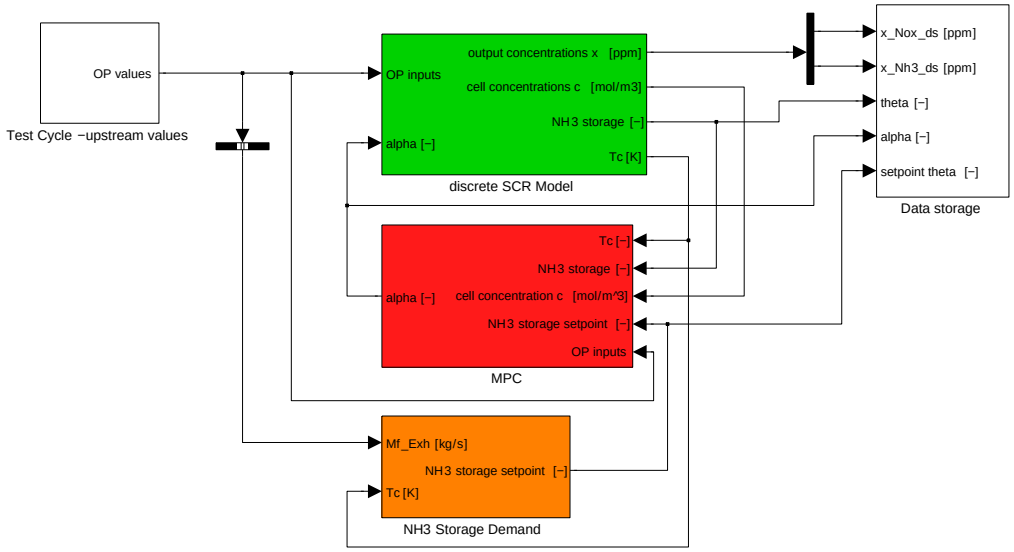


Figure 4.8.: Block diagram of principle control structure for the SCR model

with a prediction time of $T_p = 3s$. Because no integral action is included into the controller, the steady-state value of the loading is not unbiased. However, due to the weighting of the cost function, the error can be reduced by increasing the ratio of $Q/R$. The quadratic program is solved using the *quadprog* routine of MATLAB.

### 4.3.2. Simulation of 15 Cell SCR Model

As already mentioned, about 8 to 15 cells are necessary for a good approximation of the SCR model. In case of a $n$-cell SCR model, the state vector $\mathbf{x}$, input $u$ and output $y$ are defined as

$$\begin{aligned}
\mathbf{x} &= [x_1\ x_2\ x_3\ x_4\ \cdots\ x_{4n-3}\ x_{4n-2}\ x_{4n-1}\ x_{4n}]^T \\
&= [c_{NO,1}\ c_{NO2,1}\ c_{NH3,1}\ \theta_{NH3,1}\ \cdots\ c_{NO,n}\ c_{NO2,n}\ c_{NH3,n}\ \theta_{NH3,n}]^T \\
u &= \alpha \\
y &= \frac{\sum_{i=1}^{n} x_{4i}}{n}
\end{aligned} \tag{4.8}$$

where $y$ equals the mean value of the loading for $n$ cells of the SCR model.

To obtain a linear MPC for a $n$-cell SCR model, the Jacobian matrix (A.3) is augmented by $(n-1)$ rows and columns. Due to the cascaded structure of the SCR model, from the second to the last cell a systematic relation occurs. Therefore, the

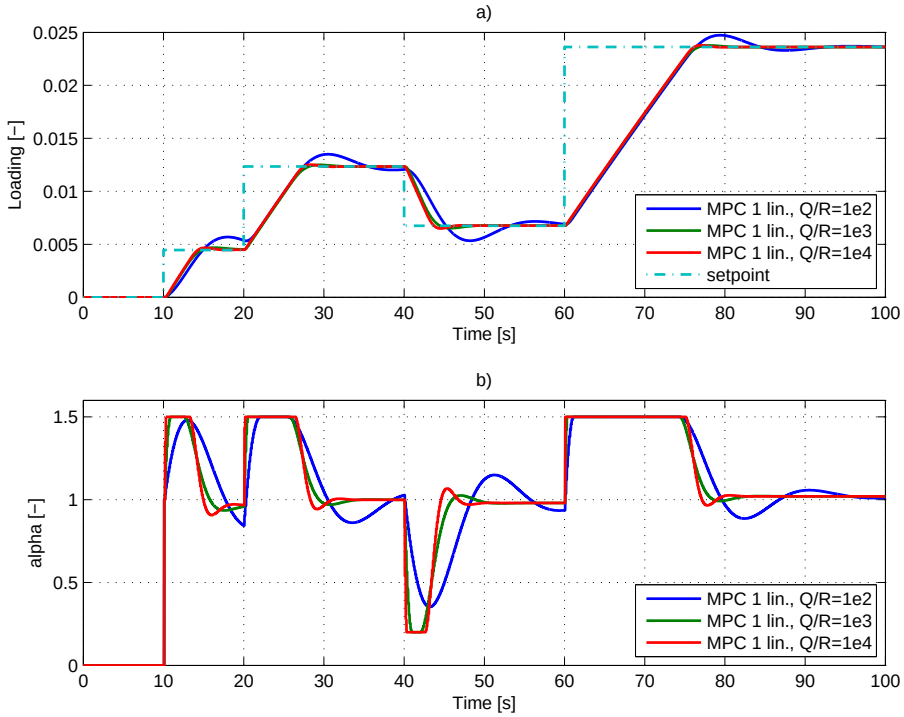


Figure 4.9.: Simulation of linear MPC for discrete SCR model with 1 cell. Different $Q/R$ ratios, $T_s = 0.1s$, $np/nc = 30/9$. a) control output, b) control action.

derivation of the Jacobian is straight forward. The explicit structure of $\mathbf{A}_c$, $\mathbf{b}_c$ and $\mathbf{c}^T$ for a 15 cell SCR model is attached in Appendix A.2.

In order to obtain the linear prediction model from the Jacobian matrix, the equilibrium of the nonlinear system has to be calculated. Due to the complexity and the high order of the system, an analytical computation of the equilibrium is not possible. Instead, the zeros of the continuous equations (2.1) have to be found by solving the system of nonlinear equations numerically. In this thesis the MATLAB routine *fsolve* is used.

Figure 4.10 depicts the simulation of the linear MPC for the 15 cell SCR model, where the linear prediction model is linearized about the equilibrium $y_e = 0.015$ near the desired loading set-point of OP7. The behavior of the controlled system is similar to the case with one 1 cell using the same sample time and horizons.

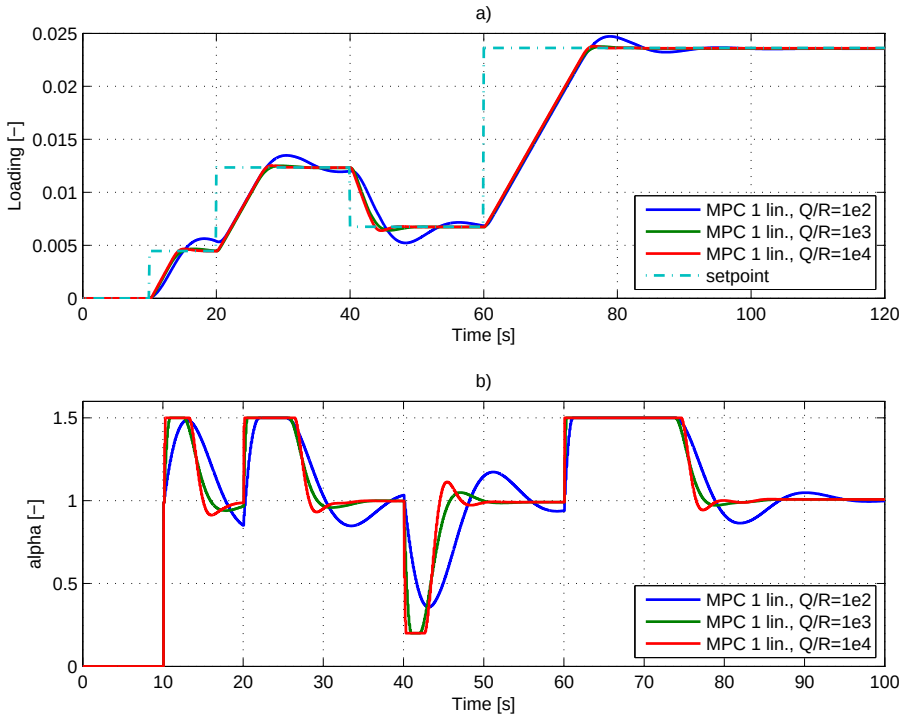


Figure 4.10.: Simulation of linear MPC for discrete SCR model with 15 cells. Different $Q/R$ ratios, $T_s = 0.1s$, $np/nc = 30/9$. a) control output, b) control action.

The linear MPC for setpoint jumps in one operating point shows a good performance for the 15 cell SCR model. In practice, the SCR system moves from one OP

to another, where the desired setpoint of the loading is depending on the current massflow of the exhausted gas $\overset{*}{m}_{EG}$ and the temperature in the catalyst $T_c$.
Figure 4.11 and 4.12 show the simulation of the linear MPC for OP jumps (OP 7-5-7 and OP 7-9-7). It can be seen that the linear MPC (linearized in OP7) has a significant loss of performance in OP9.

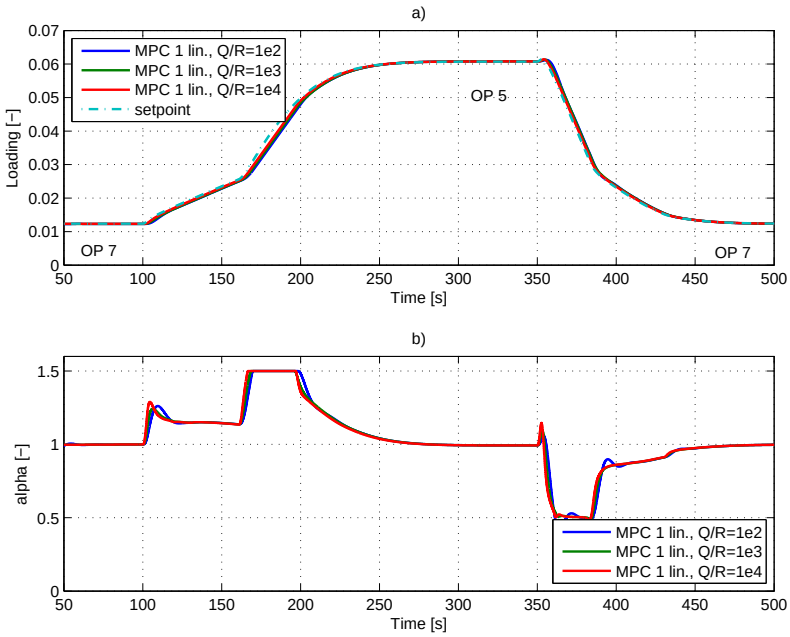


Figure 4.11.: Simulation of linear MPC for discrete SCR model with 15 cells and OP jumps 7-5-7. Different $Q/R$ ratios, $T_s = 0.1s$, $np/nc = 30/9$. a) control output, b) control action.

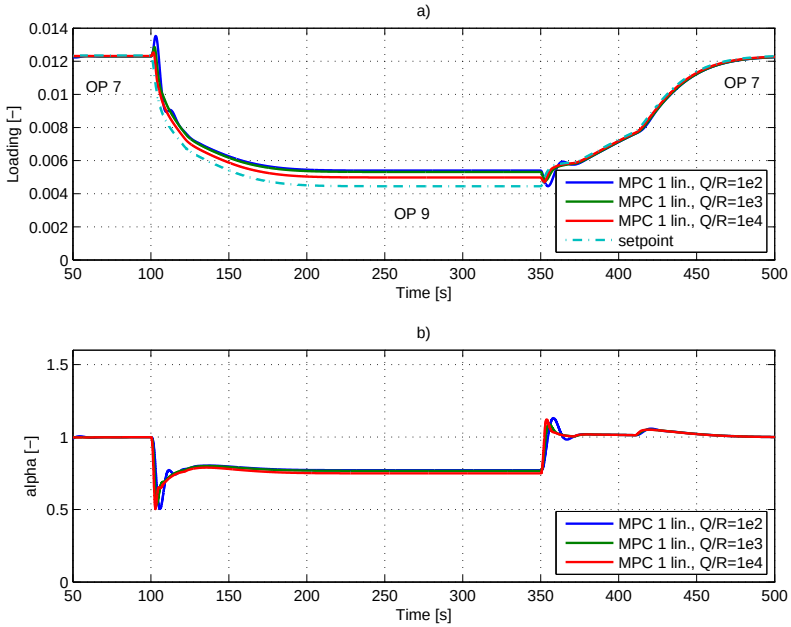


Figure 4.12.: Simulation of linear MPC for discrete SCR model with 15 cells and OP jumps 7-9-7. Different $Q/R$ ratios, $T_s = 0.1s$, $np/nc = 30/9$. a) control output, b) control action.

## 4.4. Nonlinear MPC for SCR Control of 15 Cells

A better performance in different operating points can be achieved if the prediction model of the MPC is calculated for each time step. This method is called successive linearization (SL) and is described in detail in chapter 3.3.2.
For SL using method 1 (M1), in principle the same algorithm has to be implemented as in the linear MPC case discussed before. The main difference is that the numerical calculation of the equilibrium is done for each time step or after a defined time interval and therefore the linear prediction model has to be computed online as well. As a result, the execution time increases. For a better performance of M1, it is essential to use the calculated equilibrium for each time step as starting point for the next numerical computation.
Alternatively, a second implementation of the SL is considered. Method 2 (M2) avoids the numerical computation of the equilibrium, because the nonlinear system is linearized around the current states. Additionally, an offset has to be added in this case.

Figure 4.11 and 4.12 show the comparison of the linear MPC with the nonlinear MPC using SL M1 and M2 for different OP jumps (OP 7-5-7 and OP 7-9-7). The nonlinear MPC shows a better tracking of the loading especially in high temperature

operating points (OP9). The performance of both SL methods is quite similar.

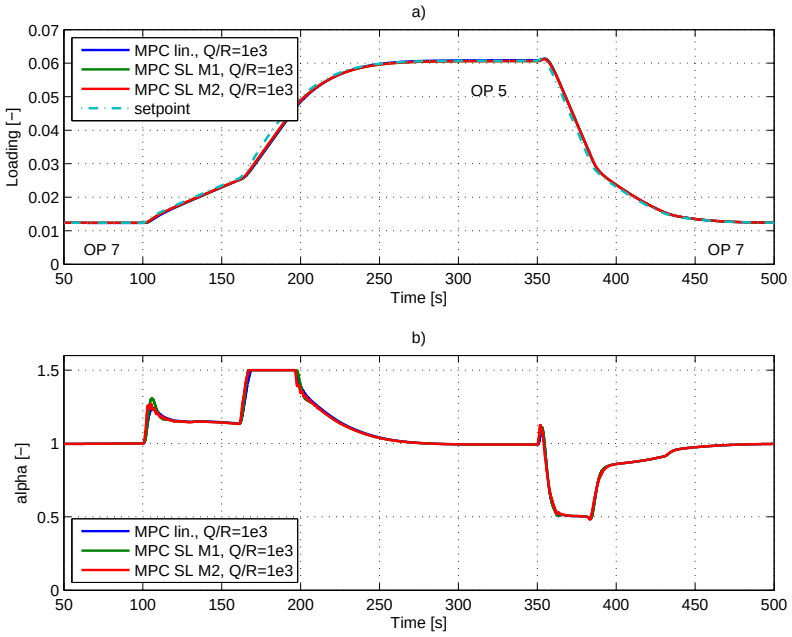


Figure 4.13.: Simulation of linear and nonlinear MPC for discrete SCR model with 15 cells and OP jumps 7-5-7. Different $Q/R$ ratios, $T_s = 0.1s$, $np/nc = 30/9$. a) control output, b) control action.

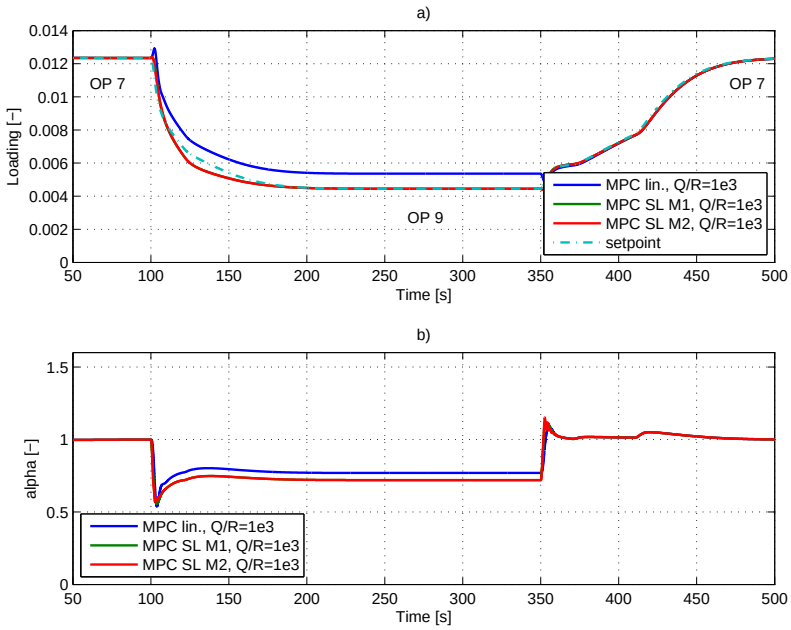


Figure 4.14.: Simulation of linear and nonlinear MPC for discrete SCR model with 15 cells and OP jumps 7-9-7. Different $Q/R$ ratios, $T_s = 0.1s$, $np/nc = 30/9$. a) control output, b) control action.

# 5. Stationary and Transient Test Cycles

In the European Union standardized test cycles for emission certifications of automotive applications and non-road mobile engines are defined. These tests include several driving conditions, for instance cold/hot starting, frequent accelerations and decelerations, changes of load, etc [12]. In order to make a realistic test in the operating range of a diesel engine, measurement data for non-road mobile diesel engines are used to test the MPC approach for the SCR system. The main input data of the so called Non-road Steady Cycle (NRSC) in parallel with the Non-road Transient Cycle (NRTC) are depicted in figure 5.1 and 5.2. The most important aspect with respect to these tests is, that the two dominant operating point values massflow $\overset{*}{m}_{EG}$ and temperature $T_{EG}$ of the exhausted gas are correlated.

## 5.1. Loading Control

### 5.1.1. NRSC Test

The following simulations include stationary test cycles with the two SLNMPC methods M1 and M2. A comparison with the standard MBC approach using a nonlinear PI controller will show the performance of the different strategies.

Figure 5.3 depicts the simulation of the NRSC test and the comparison of the nonlinear SLMPC M1, M2 and a PI control approach. The parameter $T_s$, $n_p$, $n_c$ are set as in the investigations before, the $Q/R$ ratio is $10^5$.

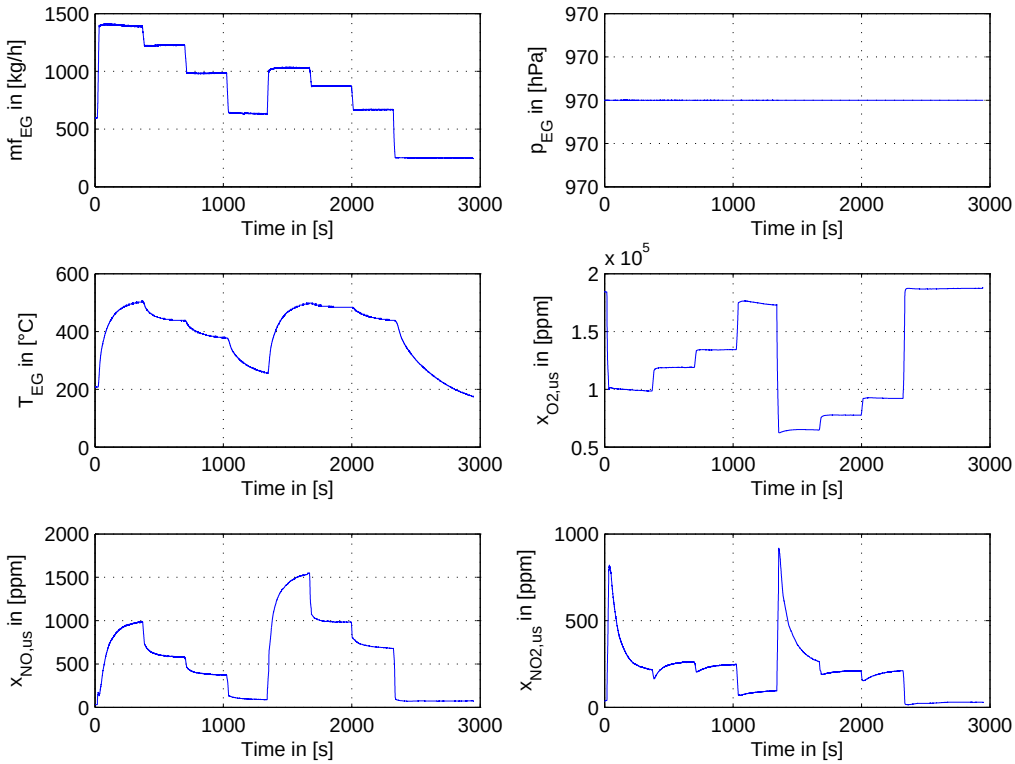


Figure 5.1.: NRSC test cycle input sequences

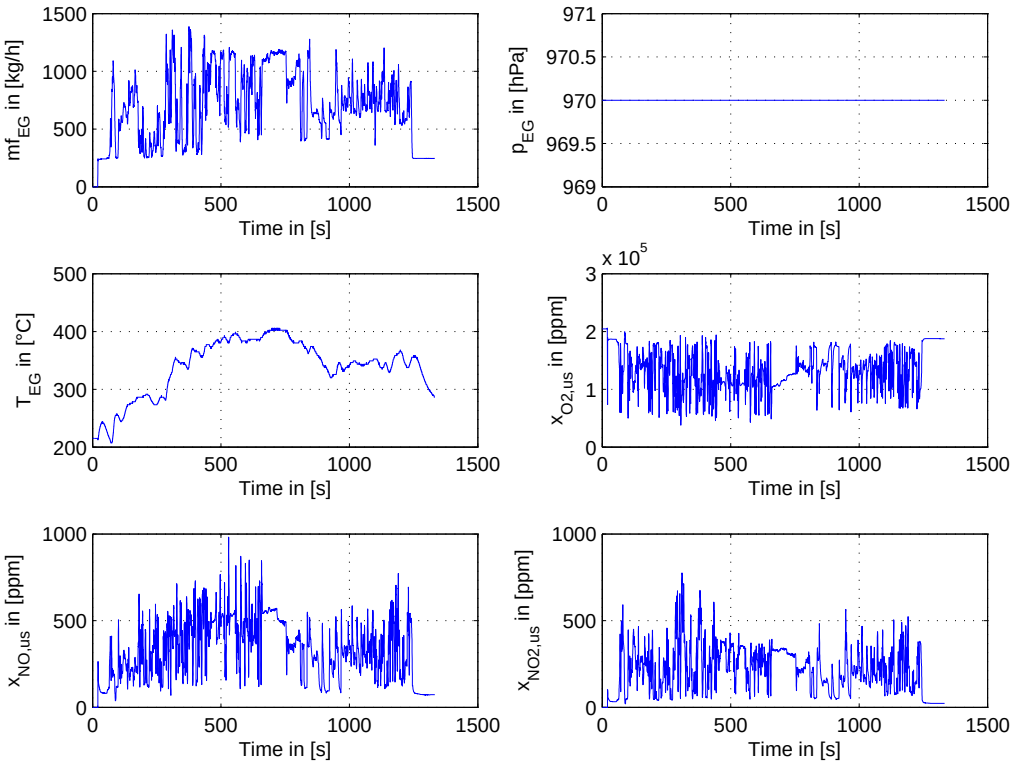


Figure 5.2.: NRTC test cycle input sequences

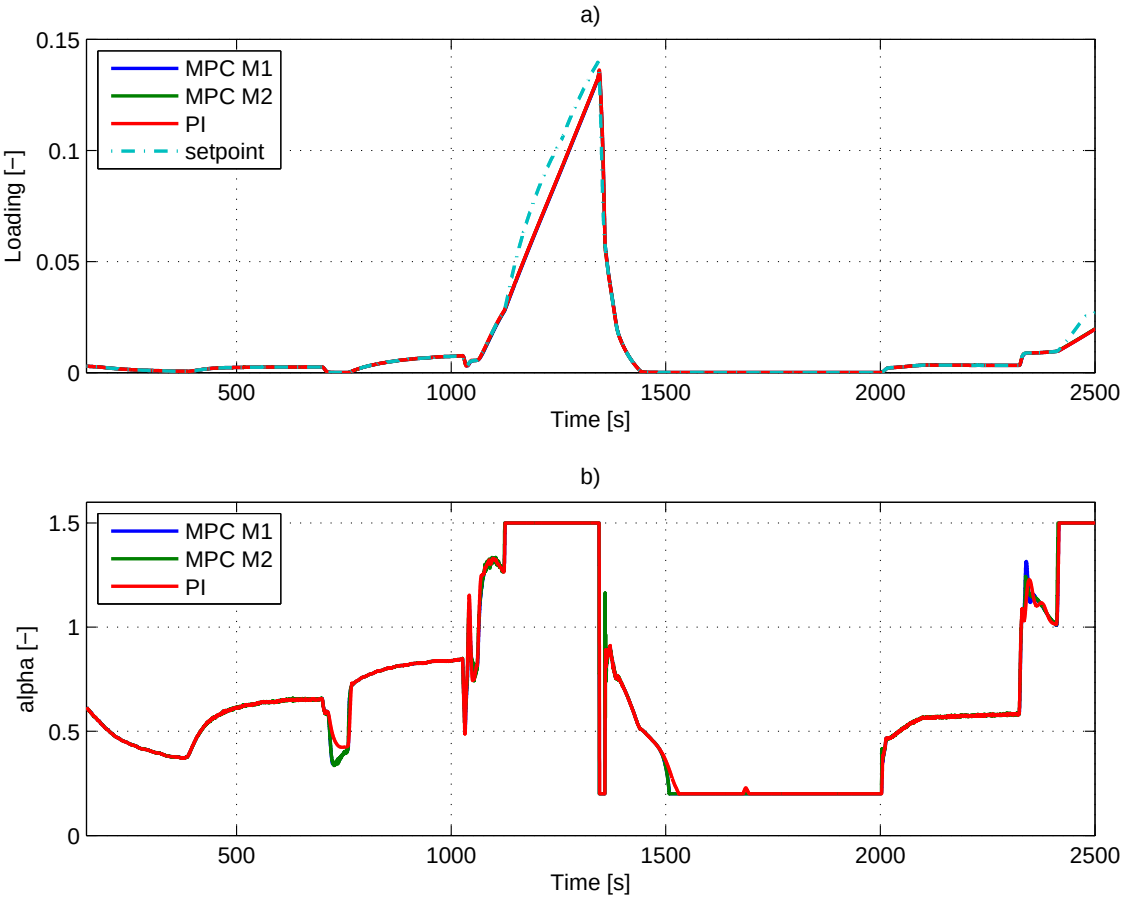


Figure 5.3.: Simulation of the NRSC test cycle for SLMPC M1,M2, and PI approach comparison, discrete SCR model with 15 cells. $Q/R = 10^5$, $T_s = 0.1s$, $np/nc = 30/9$. a) control output, b) control action.

The NRSC test is evaluated by calculating the integral absolute error (IAE) and integral squared error (ISE) of the loading as well as the integrated control action (ICA) of the feed-ratio $\alpha$. Table 5.1 presents the result for the different controller. The evaluation is considered in a time interval of [80s,2500s] due to the temperature initialization of the SCR model and a better benchmarking. All three concepts show similar performance for the stationary test. The PI has a slightly better error tracking due to the integral action but higher control activity. A higher choice of the $Q/R$-ratio reduces the error of the MPC.

| | | IAE | ISE | ICA |
|---|---|---|---|---|
| MPC SL M1 | $Q/R = 10^4$ | 3.45 | 0.0429 | 1619.4 |
| MPC SL M2 | | 3.42 | 0.0405 | 1619.9 |
| MPC SL M1 | $Q/R = 10^5$ | 3.09 | 0.0405 | 1620.1 |
| MPC SL M2 | | 3.01 | 0.0403 | 1620.2 |
| PI control | | 3.01 | 0.0408 | 1624.2 |

Table 5.1.: Calculated values of IAE, ISE and ICA of different control approaches for NRSC test cycle. $T_s = 0.1s$, $n_p/n_c = 30/9$

Figure 5.4 depicts the performance of the control concepts with respect to the emissions downstream of the catalyst. One can see that the demand map for the loading setpoint is calibrated to reach very low $NH_3$ slip but thus higher $NO_x$ emissions occur with low $DeNO_x$ ratios.

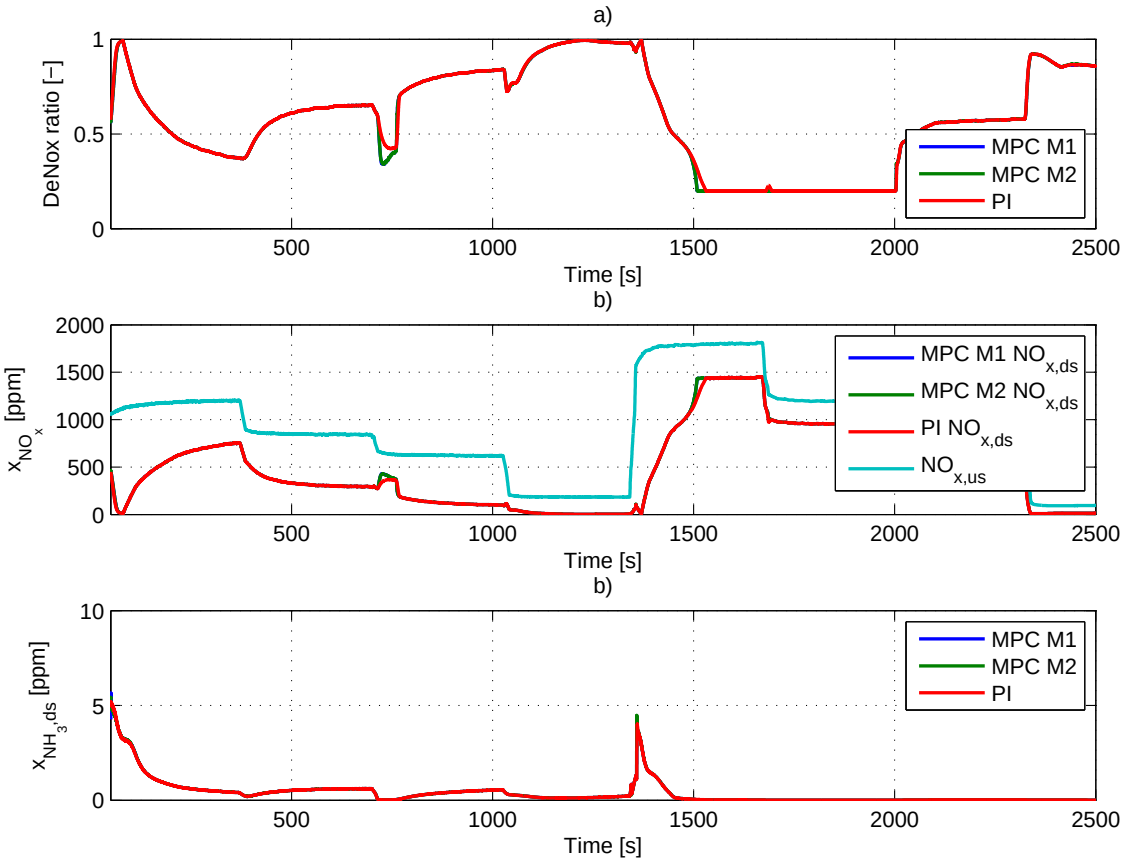


Figure 5.4.: Simulation of the NRSC test cycle for SLMPC M1,M2, and PI approach comparison, discrete SCR model with 15 cells. $Q/R = 10^5$, $T_s = 0.1s$, $np/nc = 30/9$. a) $DeNO_x$, b) $NO_{x,ds}$ c) $NH_3$ slip.

### 5.1.2. NRTC Test

The transient behavior of the nonlinear MPC using SL with M1 and M2 is evaluated in this part.

Figure 5.5 shows the simulation of the NRTC test cycle and the comparison of the nonlinear SLMPC M1, M2 and a PI control approach. The parameter $T_s$, $n_p$, $n_c$ are set as in the investigations before, the $Q/R$ ratio is $10^4$.

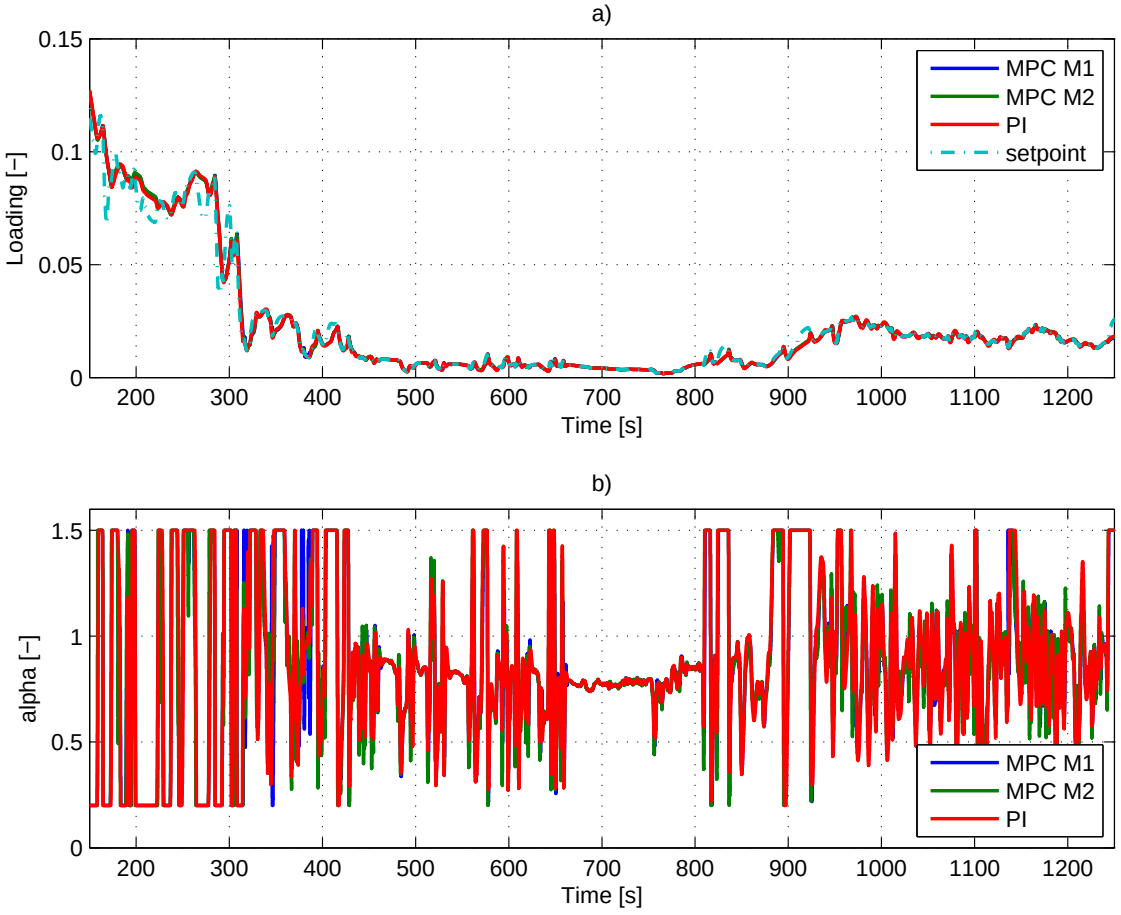


Figure 5.5.: Simulation of the NRTC test cycle for SLMPC M1,M2, and PI approach comparison, discrete SCR model with 15 cells. $Q/R = 10^4$, $T_s = 0.1s$, $np/nc = 30/9$. a) control output, b) control action.

In table 5.2 the evaluation of the NRTC test is presented. The parameter are the same as in the NRSC test. The time interval [150,1240s] is defined for the evaluation. Compared to the NRSC test, the SLNMPC shows a much better performance than the PI controller for transient conditions, especially when the ratio of $Q/R$ is

increased.

| | | IAE | ISE | ICA |
|---|---|---|---|---|
| MPC SL M1 | $Q/R = 10^4$ | 1.8310 | 0.0181 | 938.97 |
| MPC SL M2 | | 1.7905 | 0.0181 | 942.88 |
| MPC SL M1 | $Q/R = 10^5$ | 1.6552 | 0.0173 | 941.67 |
| MPC SL M2 | | 1.6686 | 0.0175 | 944.91 |
| PI control | | 1.8801 | 0.0181 | 948.05 |

Table 5.2.: Calculated values of IAE, ISE and ICA of different control approaches for NRTC test cycle. $T_s = 0.1s$, $n_p/n_c = 30/9$

In the time interval [370,390s] of the presented NRTC test, the SLNMPC M1 shows an unusual behavior, depicted in figure 5.6. The reason for these peaks in alpha are problems in the numerical computation of the equilibrium in M1. Strongly changing transient conditions from one time step to another lead to a starting point for the iteration, which is too far away to reach a reasonable solution with the implemented algorithm. Reducing the sample time or filtering the transient OP values can solve this problem.

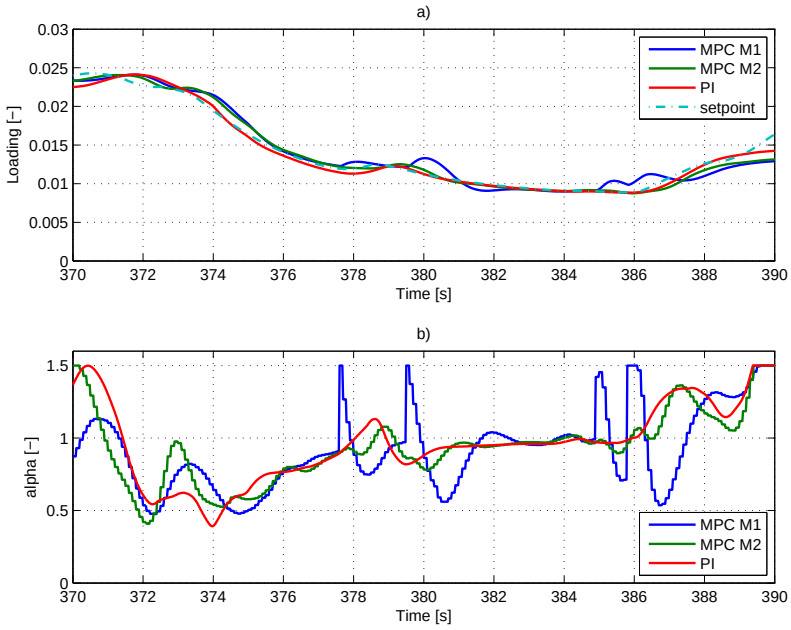


Figure 5.6.: SLMPC M1 problem in simulation of the NRTC test cycle

As a next step, the NRTC test shows how a change in the control horizon can affect the performance of the SLNMPC. In order to find an appropriate control horizon $n_c$, the SLNMPC M2 is tested for the NRTC with different horizon $n_c = [3, 6, 9, 12, 15]$. Figure 5.7 depicts the results for the IAE and computational time of the quadprog algorithm in MATLAB as a function of the control horizon. The IAE can be reduced by up to 5% with increasing $n_c$ values while ISE and ICA keep almost constant. A control horizon $n_c = 9$ seams to be a good choice. To reduce the computational time of the quadratic program, even smaller $n_c$ values are suitable.

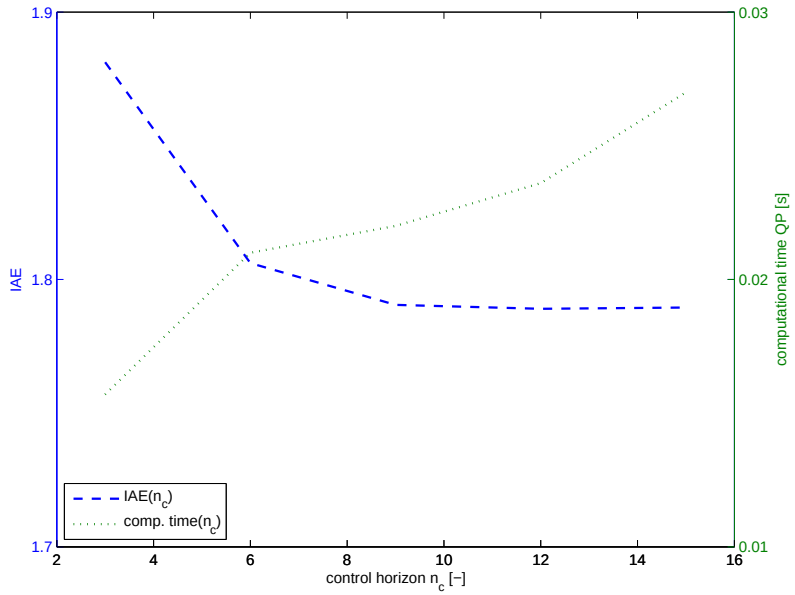


Figure 5.7.: IAE error and computational time of quadprog algorithm of SLNMPC M2 as a function of $n_c$ for NRTC test

Another aspect that has to be considered is the ratio between sample time $T_s$ of the MPC and re-linearization time $T_{lin}$ of the prediction model. Therefore, the SLNMPC M2 is evaluated for several ratios in table 5.3. It can be seen that already a small increase in the re-linearization time has an influence on the performance due to the transient operating conditions.

Figure 5.8 depicts the performance of the control concepts with respect to the exhaust gas after-treatment. Although the SLNMPC M2 controller has a superior tracking of the loading compared to the PI-controller, both concepts show similar $NO_x$ and $NH_3$ emissions. Hence, changes near the setpoint of loading have not a big influence on the emissions for this setpoint trajectory, which means that reducing the tracking error becomes less important than expected.

| $T_s/T_{lin}$ | IAE | ISE | ICA |
|---|---|---|---|
| $0.1s/1s$ | 1.7564 | 0.0177 | 943.4 |
| $0.1s/0.5s$ | 1.7116 | 0.0176 | 943.6 |
| $0.1s/0.1s$ | 1.6686 | 0.0175 | 944.9 |
| $0.08s/0.4s$ | 1.6644 | 0.0174 | 944.7 |
| $0.08s/0.08s$ | 1.6290 | 0.0172 | 945.8 |

Table 5.3.: Calculated values of IAE, ISE and ICA of SLNMPC M2 for NRTC test and varying sample/re-linearization time. $Q/R = 10^5$, $n_p/n_c = 30/9$

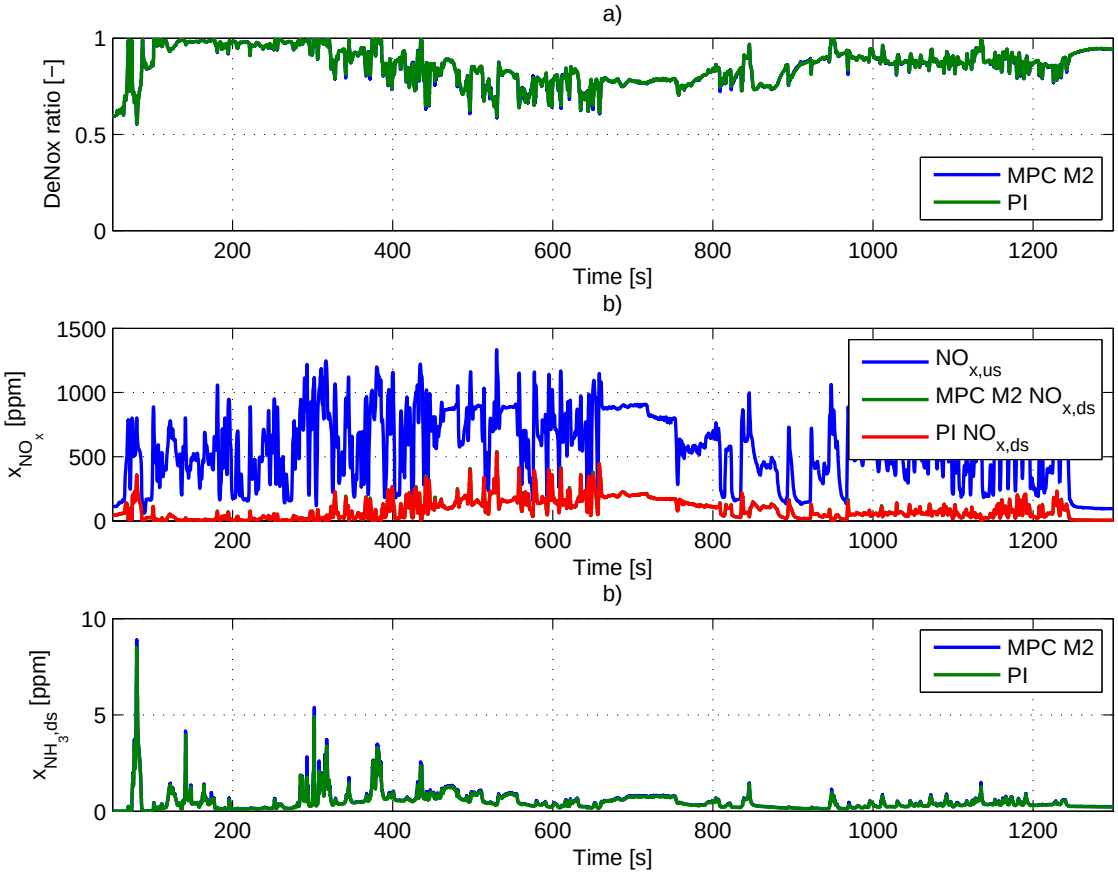


Figure 5.8.: Simulation of NRTC test for SLMPC M2 and PI approach comparison, discrete SCR model with 15 cells. $Q/R = 10^5$, $T_s = 0.1s$, $np/nc = 30/9$. a) $DeNO_x$, b) $NO_{x,ds}$ c) $NH_3$ slip.

Table 5.4 presents the corresponding mass of injected $NH_{3,us}$ upstream and the emissions $NH_{3,ds}$ and $NO_{x,ds}$ downstream of the catalyst for NRTC test conditions depicted in figure 5.8. Both concepts show similar emission quantities.

| | $m_{NH_3,us}$[g] | $m_{NH_3,ds}$[g] | $m_{NO_x,ds}$[g] |
|---|---|---|---|
| MPC SL M2 | 75.008 | 0.0819 | 24.476 |
| PI control | 74.948 | 0.0775 | 24.387 |

Table 5.4.: Calculated mass of $NO_x$ and $NH_3$ of different control approaches for NRTC test cycle

## 5.2. Efficiency Control

As seen before, the control of loading needs a lot of effort to determine the setpoint for the desired emission goals. In order to directly affect the emissions with the MPC, the $DeNO_x$ ratio (1.10) of the SCR model is set as output instead of the loading. For this control strategy, the $\mathbf{c}^T$ matrix of the linear model changes to

$$\mathbf{c}^T = -\frac{1}{c_{NO_{us}} + c_{NO_{2,us}}} \begin{bmatrix} 0 & 0 & 0 & 0 & \cdots & 1 & 1 & 0 & 0 \end{bmatrix} \tag{5.1}$$

where $\mathbf{c}^T$ has the same size as in the loading control.

Figure 5.9 and 5.10 show the $DeNO_x$ control with SLNMPC M2 compared to the PI approach with loading as output for a NRSC test. The desired setpoint is set to 90% $NO_x$ reduction. In order to reach a constant $DeNO_x$ ratio on a high level, in some OP a much higher loading is needed. Thus more $NH_3$ has to be injected and more $NH_3$ slip occurs in these operating regions.

Figure 5.11 and 5.12 show the $DeNO_x$ control with SLNMPC M2 compared to the PI approach with loading as output for a NRTC test. The desired setpoint is set to 98% $NO_x$ reduction. Compared to the loading control approach a higher control activity and loading of the catalyst can be seen. The setpoint of the loading control is defined to produce minor $NH_3$ slip. However, this results in a drop of the $DeNO_x$ efficiency in some operating regions.

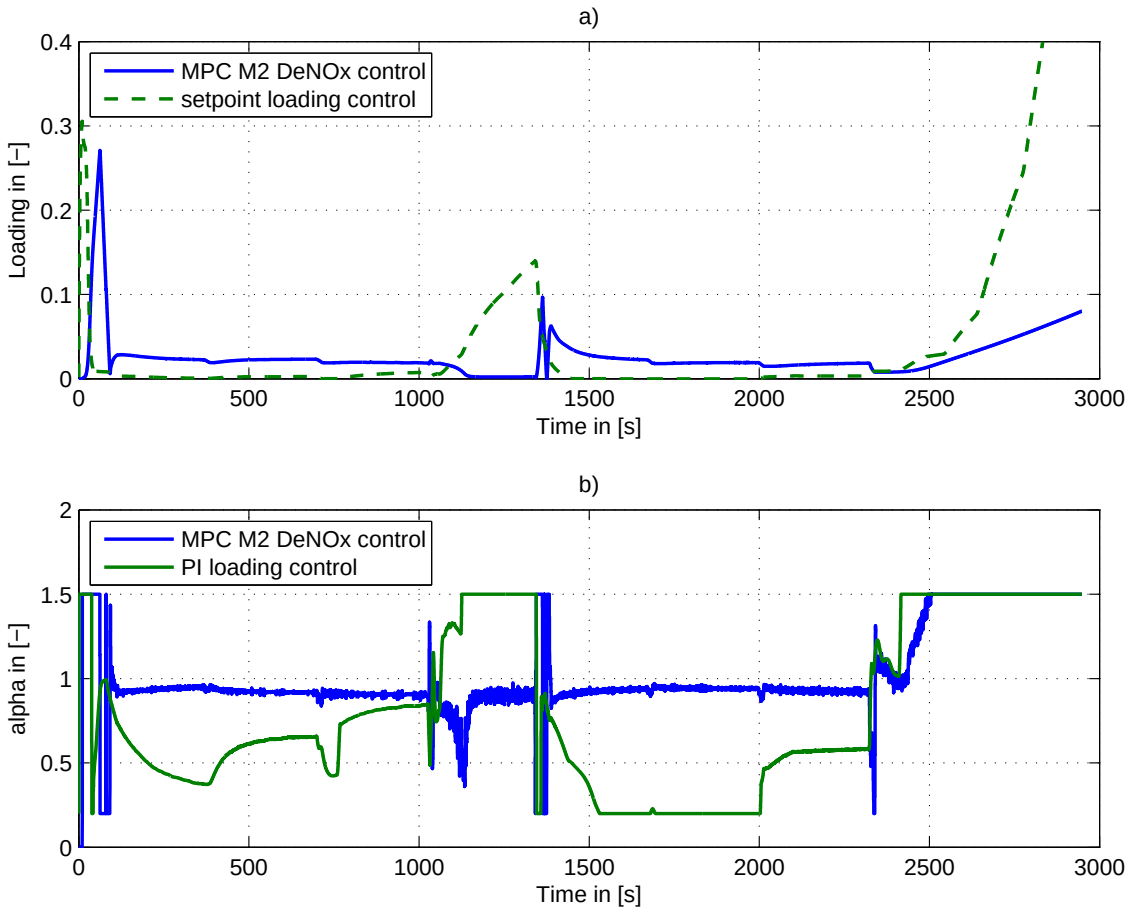


Figure 5.9.: Comparison of $DeNO_x$ control with SLNMPC M2 and loading control with nonlinear PI control for NRSC test. $Q/R = 10^2$, $T_s = 0.1s$, $np/nc = 30/9$. a) loading, b) control action

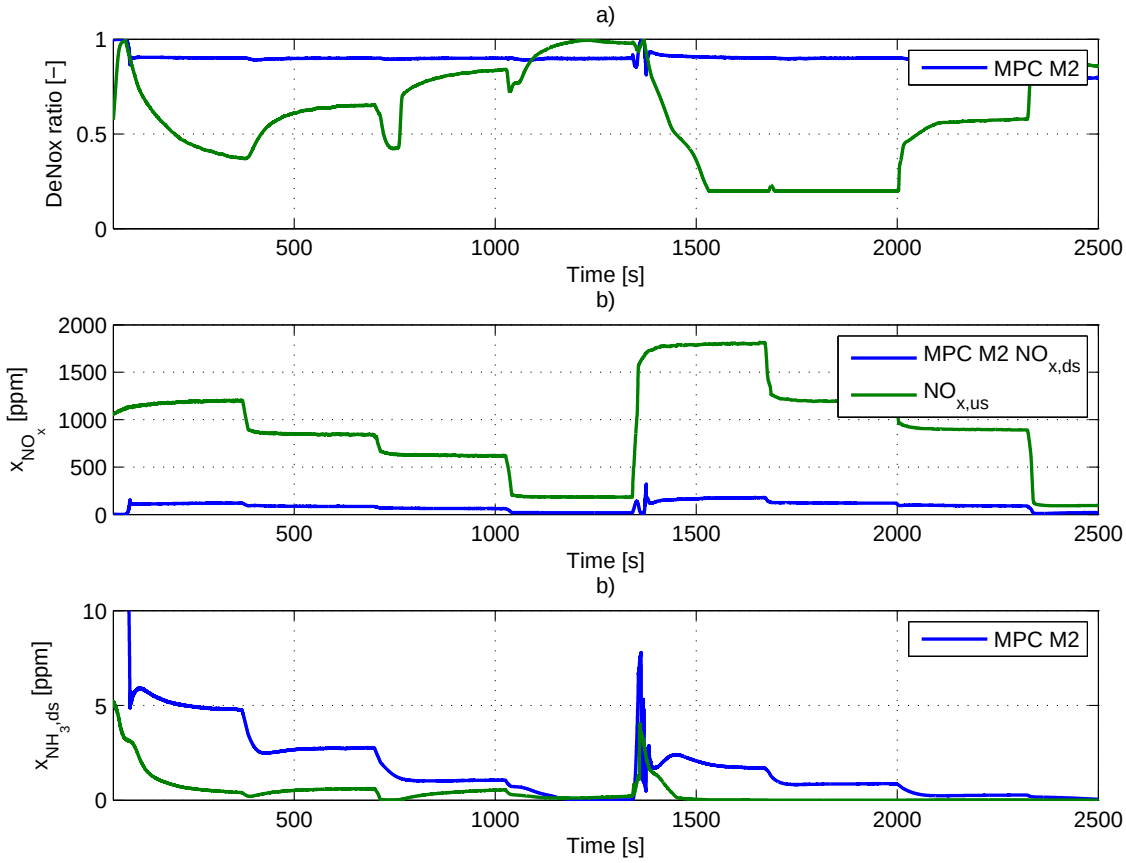


Figure 5.10.: Comparison of $DeNO_x$ control with SLNMPC M2 and loading control with nonlinear PI control for NRSC test. $Q/R = 10^2$, $T_s = 0.1s$, $np/nc = 30/9$. a) $DeNO_x$ ratio, b) $NO_{x,ds}$ c) $NH_3$ slip

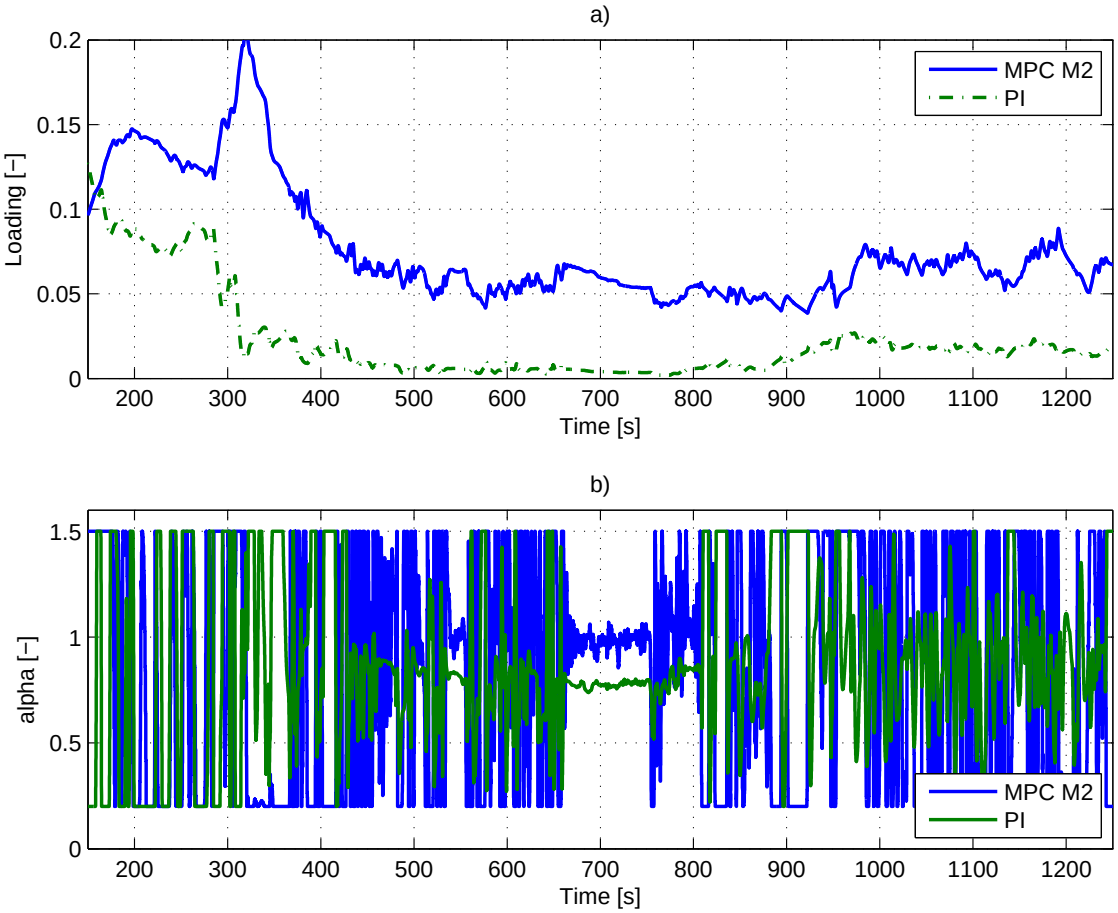


Figure 5.11.: Comparison of $DeNO_x$ control with SLNMPC M2 and loading control with nonlinear PI control for NRTC test. $Q/R = 10^2$, $T_s = 0.1s$, $np/nc = 30/9$. a) loading, b) control action

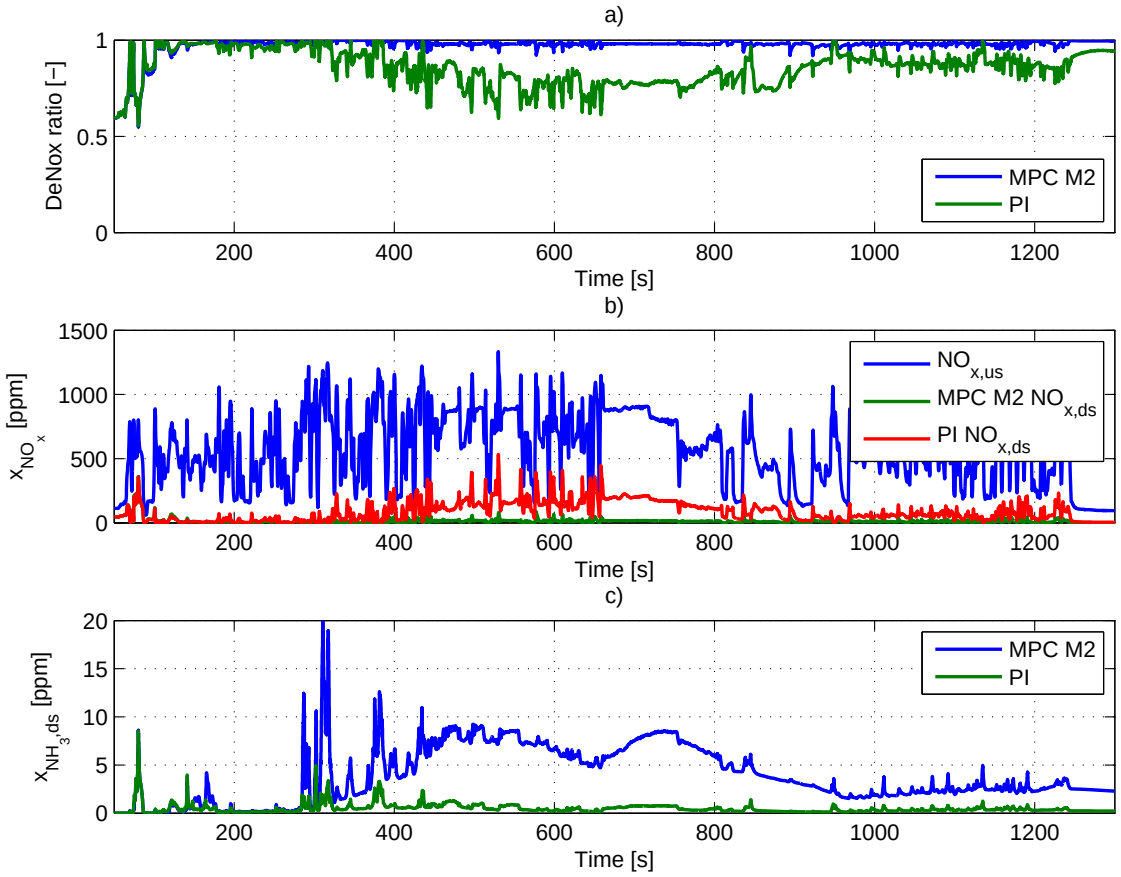


Figure 5.12.: Comparison of $DeNO_x$ control with SLNMPC M2 and loading control with nonlinear PI control for NRTC test. $Q/R = 10^2$, $T_s = 0.1s$, $np/nc = 30/9$. a) $DeNO_x$ ratio, b) $NO_{x,ds}$ c) $NH_3$ slip

The main problem of this approach is that in some OP, high amounts of ammonia are injected (overdosing) to reach the desired $DeNO_x$ ratio. Due to an ammonia slip catalyst, which converts the $NH_3$ slip downstream of the catalyst into $NO_x$, and the restriction of $NH_3$ in the emission legislation, the $NH_3$ slip has to be limited. Practically, the MPC offers a systematic implementation of constraints in state variables.
It can be seen that controlling the $DeNO_x$ ratio leads to a higher rate of change in the control action. However, the primary goal to reduce $NO_x$ emissions can be better achieved without the demand for setpoint maps of the loading. If the $NH_3$ slip is too high, a constraint of the state variable can be implemented into the MPC.

Figure 5.13 depicts the comparison of a MPC with and without a constraint of $NH_3$ downstream to 5ppm for a NRTC test. The limitation on the $NH_3$ leads to a decrease in the $DeNO_x$ efficiency. Thus, a tradeoff between the choice of $DeNO_x$ setpoint and $NH_3$ slip has to be found in this approach.

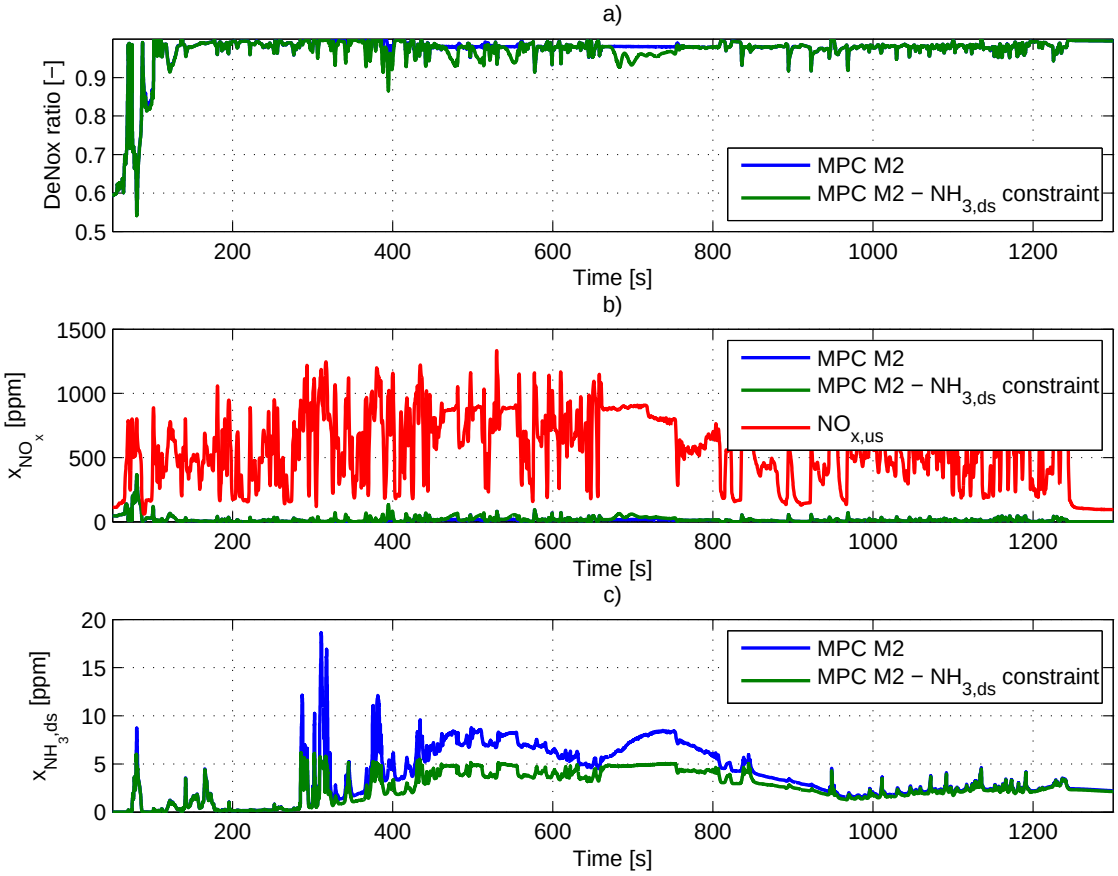


Figure 5.13.: Comparison of $DeNO_x$ control of SLNMPC M2 with and without $NH_3$ slip constraint

# 6. Conclusion and Outlook

## 6.1. Conclusion

Due to the strongly nonlinear SCR system and its wide operating range, a linear MPC algorithm was not accurate enough to control the loading of the catalyst. Therefore a nonlinear MPC, called SLNMPC, was introduced as this concept uses a re-linearized linear prediction model with quadratic optimization algorithm, which reduces the computational costs compared to other nonlinear MPC.
SLNMPC M1 is the more intuitive approach compared to M2, because an equilibrium is used for the linearization of the SCR model. However, due to the cell structure of the continuous SCR model with up to 15 cells, numerical computation of the equilibrium led to problems in transient tests. The starting point for the determination of the equilibriums was the most critical point in this concept. Hence, SLNMPC M2 using the current states from the SCR model for linearization was the preferred method. Both M1 and M2 showed similar performance, but M2 has less computational costs.

Generally speaking, the performance of the SLNMPC mainly depends on the computational effort, especially in the transient test case. The smaller the sample time $T_s$ and re-linearization time $T_{lin}$ of the MPC, the higher are the computational costs and the better is its performance. The increase of the control horizon $n_c$ up to $n_c = 9$ and thus the number of decision variables has also an influence on the tracking performance. Compared to the nonlinear PI control approach, up to 13% less IAE was achieved in the NRTC test of the loading control concept. In the stationary test cycle, no significant difference in performance of the controller could be seen. The main reason for that is that in this case, the MPC operates with less active constraints. Furthermore, the PI-controller has no offset because of the integral action. With a higher weighting of the $Q/R$ ratio in the cost function, the offset error of the MPC can be reduced. As it turned out, a better tracking of the loading than in the nonlinear PI control approach has only small affect to the $NO_x$ and $NH_3$ emissions. The main reason for that is the calculation of the demand map for the loading, which is derived from stationary points of the input/output behavior in figure 2.1. Due to the flat curve in the considered operating points, only small changes in the emissions occur.

Controlling the $DeNOx$ ratio has the advantage to directly influence the emissions downstream the SCR catalyst. A high setpoint for the efficiency leads to an overdosing of the SCR with high $NH_3$ slip. The MPC structure with state variable constraint can be used to limit the $NH_3$ downstream. Since the efficiency decreases with a stronger $NH_3$ limitation, a tradeoff between the desired $DeNOx$ rate and $NH_3$ slip has to be found. The $DeNOx$ control shows higher dynamics than the loading control, which led to more control activity.

## 6.2. Outlook

The MPC offers many possibilities for further investigations. If future trajectories of setpoint or temperature are known, the performance of the MPC could be further improved. The consideration of oxygen and temperature dependency in the prediction model would improve its accuracy, but the effect on computational time has to be observed.
Therefore the reduction of the execution time of the MPC is also a topic for future investigations. The computational time of the quadratic program could be minimized using other algorithms, such as Hildreth´s program or parallel quadratic programming. Instead of the online calculation of the prediction model, switching between linear models from defined operating points would be an alternative.
As mentioned before, the SLNMPC would be more effective and less computational expensive if the number of cells and thus the system order of the prediction model could be reduced. Therefore, changing the calibration of the SCR model to obtain an equivalent approximation of the system with less cells would be an interesting point. The effects of the MPC performance with less cells on a real SCR plant is another point.

Since controlling the kinetic part of the SCR system requires a very complex modeling with highly nonlinear equations, the consideration of the thermal part of the SCR system could be an alternative way. Therefore, a prediction model has to forecast the future trajectory of the catalyst temperature. The injection of $NH_3$ is based on the loading again, which depends on the temperature.

# A. Appendix

## A.1. Jacobian Matrices of one CSTR cell

The matrices $\mathbf{A}_c$,$\mathbf{b}_c$ and $\mathbf{c}^T$ for a 1 cell continuous linear SCR model and the loading as output are defined as:

$$\mathbf{b}_c = \begin{bmatrix} 0 \\ 0 \\ k_1 \frac{\overset{*}{m}_{EG}}{p_{EG}} (T_{EG}(c_{NO,us} + c_{NO2,us})) \\ 0 \end{bmatrix} \tag{A.1}$$

$$\mathbf{c}^T = \begin{bmatrix} 0 & 0 & 0 & 1 \end{bmatrix} \tag{A.2}$$

$$\mathbf{A}_c = \begin{bmatrix} -k_1 \frac{\overset{*}{m}_{EG}}{p_{EG}} T_c + a_R(-2k_{fst}x_{2,e}\theta_{crit}(1 - e^{-\frac{x_{4,e}}{\theta_{crit}}}) - k_{NO,I}c_{O_2}^{0.5}(1-x_{4,e})^a {x_{4,e}}^a) & a_R(-2k_{fst}x_{1,e}\theta_{crit}(1 - e^{-\frac{x_{4,e}}{\theta_{crit}}}) + \frac{k_{NO,I}}{Kequ}(1-x_{4,e})^a {x_{4,e}}^a) \\ a_R(-2k_{fst}x_{2,e}\theta_{crit}(1 - e^{-\frac{x_{4,e}}{\theta_{crit}}}) + k_{NO,I}c_{O_2}^{0.5}(1-x_{4,e})^a {x_{4,e}}^a) & -k_1 \frac{\overset{*}{m}_{EG}}{p_{EG}} T_c + a_R(-2k_{fst}x_{1,e}\theta_{crit}(1 - e^{-\frac{x_{4,e}}{\theta_{crit}}}) - \frac{k_{NO,I}}{Kequ}(1-x_{4,e})^a {x_{4,e}}^a) \\ 0 & 0 \\ \frac{1}{\Theta_{max}}(-4k_{fst}x_{2,e}\theta_{crit}(1 - e^{-\frac{x_{4,e}}{\theta_{crit}}}) & \frac{1}{\Theta_{max}}(-4kfstx_{1,e}\theta_{crit}(1 - e^{-\frac{x_{4,e}}{\theta_{crit}}}) \end{bmatrix} \tag{A.3}$$

$$\begin{bmatrix} 0 & a_R(-2k_{fst}x_{1,e}x_{2,e}e^{-\frac{x_{4,e}}{\theta_{crit}}} - k_{NO,I}(x_{1,e}c_{O_2}^{0.5} - \frac{x_{2,e}}{Kequ})(-a(1-x_{4,e})^{a-1}{x_{4,e}}^a + a(1-x_{4,e})^a(x_{4,e})^{a-1}) \\ 0 & a_R(-2k_{fst}x_{1,e}x_{2,e}e^{-\frac{x_{4,e}}{\theta_{crit}}} + k_{NO,I}(x_{1,e}c_{O_2}^{0.5} - \frac{x_{2,e}}{Kequ})(-a(1-x_{4,e})^{a-1}{x_{4,e}}^a + a(1-x_{4,e})^a(x_{4,e})^{a-1}) \\ -k_1 \frac{\overset{*}{m}_{EG}}{p_{EG}} T_c + a_R(-k_{ad} + k_{ad}x_{4,e} - 4k_{ox,g}) & a_R(k_{ad}x_{4,e} + k_{de}) \\ \frac{1}{\Theta_{max}}(k_{ad} - k_{ad}x_{4,e}) & \frac{1}{\Theta_{max}}(-k_{ad}x_{3,e} - k_{de} - 4k_{fst}x_{1,e}x_{2,e}e^{-\frac{x_{4,e}}{\theta_{crit}}} - 4k_{ox}) \end{bmatrix}$$

The standard and slow SCR reactions are not considered in this linearization.

## A.2. Jacobian Matrices of n CSTR cells

Matrix $\mathbf{A}_{c1}$ is defined as Jacobian matrix (A.3) of the first CSTR cell. For the following cells, $\mathbf{A}_{c2}, .., \mathbf{A}_{cn}$ have the same form as $\mathbf{A}_{c1}$, but with their corresponding equilibriums. For example, matrix $\mathbf{A}_{cn}$ uses $x_{4(n-1)+1,e}$ to $x_{4(n-1)+4,e}$, where $n$ is the cell number.

The matrices $\mathbf{A}_c$,$\mathbf{b}_c$ and $\mathbf{c}^T$ for n cells are then defined as:

$$\mathbf{A}_{c(4\text{n x }4\text{n})} = \begin{bmatrix} \mathbf{A}_{c1} & \mathbf{0} & \mathbf{0} & \mathbf{0} & \cdots & \mathbf{0} \\ \mathbf{A}_{-1} & \mathbf{A}_{c2} & \mathbf{0} & \mathbf{0} & \cdots & \mathbf{0} \\ \mathbf{0} & \mathbf{A}_{-1} & \mathbf{A}_{c3} & \mathbf{0} & \cdots & \mathbf{0} \\ \vdots & \ddots & \ddots & \ddots & \ddots & \vdots \\ \mathbf{0} & \cdots & \mathbf{0} & \mathbf{A}_{-1} & \mathbf{A}_{cn-1} & \mathbf{0} \\ \mathbf{0} & \cdots & \mathbf{0} & \mathbf{0} & \mathbf{A}_{-1} & \mathbf{A}_{cn} \end{bmatrix} \tag{A.4}$$

$$\mathbf{b}_{c(1\text{ x }4\text{n})} = \begin{bmatrix} 0 \\ 0 \\ k_1 \frac{\overset{*}{m}_{EG}}{p_{EG}} (T_{EG}(c_{NO,us} + c_{NO2,us})) \\ 0 \\ \vdots \\ 0 \end{bmatrix} \tag{A.5}$$

$$\mathbf{c}^T_{(4\text{n x }1)} = \frac{1}{n} \begin{bmatrix} 0 & 0 & 0 & 1 & \cdots & 0 & 0 & 0 & 1 \end{bmatrix} \tag{A.6}$$

with

$$\mathbf{A}_{-1} = \begin{bmatrix} k_1 \frac{\overset{*}{m}_{EG}}{p_{EG}} T_c & 0 & 0 & 0 \\ 0 & k_1 \frac{\overset{*}{m}_{EG}}{p_{EG}} T_c & 0 & 0 \\ 0 & 0 & k_1 \frac{\overset{*}{m}_{EG}}{p_{EG}} T_c & 0 \\ 0 & 0 & 0 & 0 \end{bmatrix}, \mathbf{0} = \begin{bmatrix} 0 & 0 & 0 & 0 \\ 0 & 0 & 0 & 0 \\ 0 & 0 & 0 & 0 \\ 0 & 0 & 0 & 0 \end{bmatrix}$$

# Bibliography

[1] Bamimore, A., O. Taiwo, and R. King: *Comparison of two nonlinear model predictive control methods and implementation on a laboratory three tank system.* In *2011 50th IEEE Conference on Decision and Control and European Control Conference*, pages 5242–5247, Dec 2011.

[2] Bartsch, H.J.: *Taschenbuch mathematischer Formeln.* Fachbuchverl. Leipzig im Carl-Hanser-Verl, 2007.

[3] Bemporad, A.: *Model predictive control: Basic concepts @ONLINE*, July 2016. http://www.seas.upenn.edu/.

[4] Camacho, E.F. and C. Bordons: *Model Predictive Control.* Springer, 2007.

[5] Candau, Rafael: *Function documentation - DocMdl.* AVL internal research, 2016. DocMdl.pdf.

[6] Cartus, Thomas: *TECHNICAL TRAININING - PTE EXHAUST AFTERTREATMENT.* AVL internal research, 2013. TC_DE_2013-03-27-Academy-Aftertreatment-Training_HO.pdf.

[7] Engeljehringer, Kurt: *Emission: Heavy duty and off-road @ONLINE*, July 2016. https://www.avl.com/documents/10138/1027860/AVL+Emission+-+Applications+-+Heavy-Duty+and+Off-Road+-+2014-10-12.pdf/56c9a2c9-1174-4b45-8907-0214c20966fd.

[8] Hollauf, Bernd: *Model-Based Closed-Loop Control of SCR Based DeNOx Systems.* Master's thesis, University of Applied Science Technikum Kaernten, 2009.

[9] Horn, M. and N. Dourdoumas: *Regelungstechnik.* Pearson, 2004.

[10] Maciejowski, J.M.: *Predictive Control with Constraints.* Pearson Education Limited, 2002.

[11] Nova, Isabella: *Urea-SCR technology for deNOx after treatment of diesel exhausts.* Springer, 2014.

[12] Rakopoulos, Constantine: *Diesel engine transient operation principles of operation and simulation analysis.* Springer, 2009.

[13] Reif, Konrad: *Dieselmotor-Management Systeme, Komponenten, Steuerung und Regelung*. Vieweg+Teubner Verlag, 2012.

[14] Schär, Christoph: *Control of a selective catalytic reduction process*. IMRT Press c/o Institut für Mess- und Regeltechnik, ETH Zentrum, Zürich, 2003.

[15] Wabnig, Armin: *SCR SW TRAINING INTRODUCTION*. AVL internal research, 2015. B634487_SCR_SW_Training_Workshop_Introduction_AWA.pdf.

[16] Wang, Liuping: *Model predictive control system design and implementation using MATLAB*. Springer, London, 2009, ISBN 978-1-84882-331-0.

[17] Willems, Frank: *Is closed-loop SCR control required to meet future emission targets?* SAE international 2007-01-1574, 2007.